AGU PUBLICATIONS

Paleoceanography

RESEARCH ARTICLE
10.1002/2014PA002710

Key Points:
- Last Interglacial started within 1000 years or less
- Younger Dryas-type rebound occurred during last interglacial
- Continuing ice melt delayed full interglacial conditions by several millennia

Supporting Information:
- Figures S1–S5

Correspondence to:
P. Jiménez-Amat and R. Zahn,
pjamat@gmail.com;
rainer.zahn@uab.cat

Citation:
Jiménez-Amat, P., and R. Zahn (2015), Offset timing of climate oscillations during the last two glacial-interglacial transitions connected with large-scale freshwater perturbation, *Paleoceanography*, *30*, 768–788, doi:10.1002/2014PA002710.

Received 20 AUG 2014
Accepted 20 MAY 2015
Accepted article online 26 MAY 2015
Published online 24 JUN 2015

Offset timing of climate oscillations during the last two glacial-interglacial transitions connected with large-scale freshwater perturbation

Patricia Jiménez-Amat[1,2] and Rainer Zahn[1,3]

[1]Institute of Environmental Science and Technology, Universitat Autònoma de Barcelona, Bellaterra, Spain, [2]Now at SGS Group Spain, Madrid, Spain, [3]Institució Catalana de Recerca i Estudis Avançats, Departament de Física, Universitat Autònoma de Barcelona, Bellaterra, Spain

Abstract Multidecadal to centennial planktic $\delta^{18}O$ and Mg/Ca records were generated at Ocean Drilling Program Site 976 (ODP976) in the Alboran Sea. The site is in the flow path of Atlantic inflow waters entering the Mediterranean and captured North Atlantic signals through the surface inflow and the atmosphere. The records reveal similar climatic oscillations during the last two glacial-to-interglacial transitions, albeit with a different temporal pacing. Glacial termination 1 (T1) was marked by Heinrich event 1 (H1), post-H1 Bølling/Allerød warming, and Younger Dryas (YD) cooling. During T2 the H11 $\delta^{18}O$ anomaly was twice as high and lasted 30% longer than during H1. The post-H11 warming marked the start of MIS5e while the subsequent YD-style cooling occurred during early MIS5e. The post-H11 temperature increase at ODP976 matched the sudden Asian Monsoon Termination II at 129 ka B.P. Extending the ^{230}Th-dated speleothem timescale to ODP976 suggests glacial conditions in the Northeast Atlantic region were terminated abruptly and interglacial warmth was reached in less than a millennium. The early-MIS5e cooling and freshening at ODP976 coincided with similar changes at North Atlantic sites suggesting this was a basin-wide event. By analogy with T1, we argue that this was a YD-type event that was shifted into the early stages of the last interglacial period. This scenario is consistent with evidence from northern North Atlantic and Nordic Sea sites that the continuing disintegration of the large Saalian Stage (MIS6) ice sheet in Eurasia delayed the advection of warm North Atlantic waters and full-strength convective overturn until later stages of MIS5e.

1. Introduction

The glacial-interglacial climatic transitions of the Pleistocene constituted the largest naturally sustained climate change scenarios of the recent geologic past. They involved large-scale freshwater perturbation near the centers of convection in the northern North Atlantic and hence they serve as a natural reference for modeling the possible impacts of growing marine freshwater budgets under concurrent global warming [*Schmittner and Galbraith*, 2008; *Jackson et al.*, 2010; *Clark et al.*, 2012; *Liu et al.*, 2013; *Mohtadi et al.*, 2014]. The last interglacial Marine Isotope Stage (MIS) 5e likewise attracts the attention of the climate modeling and prediction community because higher-orbital eccentricity and a more negative precession index caused solar radiative forcing to be higher than preindustrial levels hence mimicking anticipated future anthropogenically caused greenhouse gas forcing [*Berger and Loutre*, 2002; *Masson-Delmotte et al.*, 2006; *Stouffer et al.*, 2006; *Otto-Bliesner et al.*, 2006; *van de Berg et al.*, 2011; *Yin and Berger,* 2011; *Bakker et al.*, 2013].

Proxy-based paleoclimatic studies demonstrated that the last two glacial periods ended with several large-scale climatic oscillations that were triggered by pulsed meltwater injections to the North Atlantic from the disintegrating circum-North Atlantic ice sheets [*Rasmussen et al.*, 2006; *Carlson*, 2008; *Deschamps et al.*, 2012; *Carlson and Clark*, 2012; *Nicholl et al.*, 2012; *Martrat et al.*, 2014]. Notable examples were the Heinrich events 1 and 11 (H1 and H11) during the early phases of T1 and T2 that caused widespread cooling across the North Atlantic [*McManus et al.*, 1994; *Cayre et al.*, 1999; *Skinner et al.*, 2003; *Bard et al.*, 2000; *Oppo et al.*, 2006; *Skinner and Shackleton*, 2006; *Toucanne et al.*, 2010; *Soulet et al.*, 2013]. The Bølling/Allerød warm excursion and subsequent Younger Dryas (YD) cold spell during T1 constituted what by now are archetypal case examples of the climatic impacts connected with freshwater modulation of the North Atlantic overturning circulation and ensuing changes of poleward marine heat transports [*Condron*

and Winsor, 2012; *Jackson et al.*, 2010; *Clark et al.*, 2012; *Liu et al.*, 2013; *Mohtadi et al.*, 2014]. To date, it remains unresolved if a similar climatic oscillation existed during T2. The subsequent interglacial climates of the Holocene and MIS5e were marked by climatic transients such as the 8.2 kyr event during the early Holocene and similar cold excursions during MIS5 that propagated to the deep ocean highlighting the impacts of the climatic instability for convective activity and deep water circulation [*Bond et al.*, 2001; *Oppo et al.*, 2006; *Carlson et al.*, 2008; *Wanner et al.*, 2011; *Bauch et al.*, 2012; *Bauch*, 2013; *Sánchez-Goñi et al.*, 2013; *Galaasen et al.*, 2014].

The significance of these paleoclimatic developments for the wider North Atlantic region and in fact, the Northern Hemisphere at large became apparent from European and Chinese speleothem profiles. δ^{18}O profiles from speleothems in Mediterranean Europe and Israel [*Bard et al.*, 2002; *Bar-Matthews et al.*, 2003; *Genty et al.*, 2003; *Bar-Matthews and Ayalon*, 2004; *Drysdale et al.*, 2005, 2007; *Couchoud et al.*, 2009; *Drysdale et al.*, 2009; *Grant et al.*, 2012] displayed transient oscillations that showed remarkably good correspondence with paleoceanographic reconstructions at the western Iberian Margin and with European pollen sequences, highlighting the connection of western European climatic variability with the marine heat budgets of the North Atlantic and Mediterranean Sea [*Bar-Matthews et al.*, 2003; *Drysdale et al.*, 2009; *Sánchez-Goñi et al.*, 2012, 2013]. Correlation with Asian speleothem δ^{18}O records of monsoon variability indicated far-field teleconnections between North Atlantic heat budgets and the dominant orbital precession forcing of the monsoons and North Indian Ocean surface temperatures [*Wang et al.*, 2001; *Yuan et al.*, 2004; *Wang et al.*, 2005; *Cheng et al.*, 2006; *Kelly et al.*, 2006; *Cheng et al.*, 2009; *Pausata et al.*, 2011; *Li et al.*, 2014]. Paleoceanographic profiles from the northern North Atlantic and the Nordic Seas compellingly demonstrated that while interglacial warmth and full-strength deep water convection was established at the onset of the Holocene, it was delayed during the penultimate climatic transition until mid-MIS5e, i.e., several millennial after the onset of interglacial climates globally [*Van Nieuwenhove et al.*, 2011; *Bauch*, 2013; *Van Nieuwenhove et al.*, 2013].

We present new high-resolution profiles of planktic δ^{18}O and Mg/Ca temperatures from Ocean Drilling Program (ODP) Site 976 in the Alboran Sea, westernmost Mediterranean Sea, to elucidate the surface climatology during the last two glacial-interglacial transitions from the perspective of the midlatitude North Atlantic. ODP976 is located immediately east of the Strait of Gibraltar [*Comas et al.*, 1996; *Zahn et al.*, 1999] in the pathway of the Atlantic water inflow that compensates for the negative water balance of the Mediterranean Sea that is driven by excess evaporation over its eastern basin [*Rohling et al.*, 2009]. The site receives the paleoclimatic signals of the North Atlantic region with these inflow waters and through the atmosphere, and the elevated sediment deposition rates at ODP 976 provided the possibility to sample the paleovariability of the North Atlantic climatology at multidecadal to centennial scales. The δ^{18}O and Mg/Ca temperature profiles display a strikingly similar sequence of events during both transitions while the timing of the events is different, highlighting the different melting histories of the large ice sheets surrounding the northern North Atlantic and Nordic Seas. The ODP976 records help to shed light on the so far controversially discussed issue [*Carlson*, 2008; *Bauch et al.*, 2012; *Sánchez-Goñi et al.*, 2013] if climatic oscillations like the Bølling/Allerød and Younger Dryas that feature prominently during T1 also existed during T2.

2. Materials and Methods

2.1. ODP Site 976 Location and Core Sampling

The surface hydrology at ODP Site 976 (36°12′N, 004°18′W, 1108 m water depth) is defined by the entrance of a 200–300 m thick Atlantic inflow layer entering the western Alboran Sea through the Strait of Gibraltar (Figure 1). In situ instrumental hydrographic data from the MEDARGroup/MEDATLAS database (2002, http://www.ifremer.fr/medar/cdrom_database.htm.) display an average annual surface salinity in the Alboran Sea of 36.5 practical salinity unit (psu) and an average annual sea surface temperature (SST) of 18°C. The full temperature range over the whole year is between 15°C in February and 23°C in August; average fall and spring SSTs are 18°C and 17°C. Initial stratigraphic and palaeoceanographic work demonstrated the continuity of multiple offset-drilled hydraulic piston cores that were recovered during ODP Leg 161 at Site 976 [*Zahn et al.*, 1999] and revealed high sedimentation rates at the Site of $>$20 cm/kyr [*Combourieu-Nebout et al.*, 1999; *de Kaenel et al.*, 1999; *Serrano et al.*, 1999; *von Grafenstein et al.*, 1999].

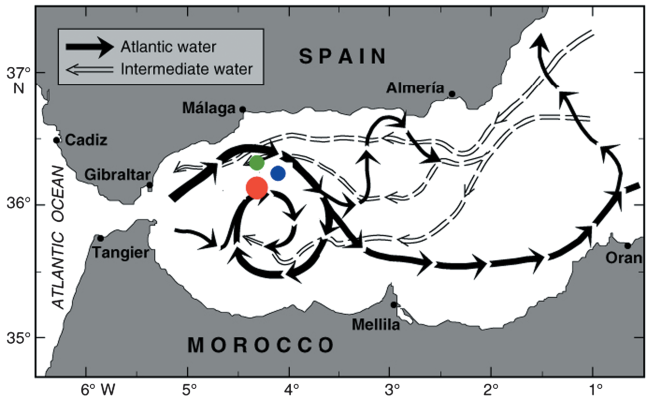

Figure 1. Surface and intermediate water circulation in the Alboran Sea and location of Site 976 and core tops considered for our calibration. Arrows schematically indicate mean trajectories of surface (solid arrows) and deep (open arrows) water circulation. Red dot marks ODP 976 location; green and blue dots mark sites Alb-1 and T-1 that are used to cross-check the ODP976 Mg/Ca temperature calibration [*Masqué et al.*, 2003, I. Cacho, personal communication]. Modified from *Combourieu-Nebout et al.* [1999].

For this study we sampled over 18 m of core sections at 2 cm intervals (Table 1) at the IODP Bremen Core Repository, Germany, yielding a total of 943 samples of which 486 samples covered the MIS2-T1-Holocene sequence (25 kyr to recent) and 457 samples the MIS6-T2-MIS5e sequence (146–104 kyr). A composite depth scale was available from Holes B–D from matching gamma ray attenuation porosity evaluator density, magnetic susceptibility, natural gamma radiation, and 550 nm wavelength color reflectance records of the three holes [*Comas et al.*, 1996] and was used to place all samples on a unified depth scale (meters composite depth, mcd) before developing the age models for the two stratigraphic sequences.

2.2. Sample Preparation

An ideal number of 30–40 specimens of planktonic foraminifera *Globigerina bulloides* was picked from the 250–315 μm size fraction to accommodate the carbonate volume needed for paired $\delta^{18}O$ and Mg/Ca analysis. However, 55% of the samples across the MIS2-T1-Holocene sequence and 34% of the samples across the MIS6-T2-MIS5e sequence yielded smaller numbers of specimens so that in these cases adjacent samples were combined or the limited number of specimens was used for either trace element or oxygen isotope analysis. Prior to analysis the foraminiferal shells were carefully crushed between methanol-cleaned glass slides to break open individual chambers in order to release possible sediment filling and support an efficient cleaning of the samples. From the crushed material, approximately one fourth of the sample was used for stable isotope measurements and the rest for trace element analyses.

2.3. Stable Isotope Analysis

A total of 884 stable isotope measurements were carried out, including 184 replicates that were measured if foraminifera abundance permitted, 329 analyses covering the MIS2-T1-Holocene section, and 371 covering the MIS6-T2-MIS5e sequence. Around 30 μg of crushed homogenized calcite per sample was cleaned by means of consecutive methanol rinses and brief sonications to remove clays and other possible sedimentary components from the sample. Measurements were conducted with a Thermo Scientific MAT253 Isotope Ratio Mass Spectrometer coupled to a Kiel IV sample gas preparation device. To monitor data quality and possible instrument drift, the International Atomic Energy Agency CO-1 carbonate standard was measured, typically every tenth sample, which amounted to four analyses of carbonate standard per batch of 36 samples. Based on 349 analyses of this carbonate standard, external reproducibility was better than 0.08 for $\delta^{18}O$.

2.4. Trace Element Analysis

A total of 514 Mg/Ca ratios were measured, 232 for the MIS2-T1-Holocene sequence and 282 for the MIS6-T2-MIS5e sequence. The cleaning protocol followed *Boyle* [1983] and *Boyle and Keigwin* [1985], implementing modifications developed in *Barker et al.* [2003] and *Pena et al.* [2005]. Foraminiferal samples first underwent repeated rinses with ultra-purified water (milli-Q) and methanol combined with brief sonication in order to remove clay minerals. To remove potential contaminant phases such as Mn-Fe-oxide a reductive reagent

Table 1. ODP976 Drill Holes and Sections Within Holes Sampled for This Study

Sequence	Hole	Depth[a] (mbsf)	Depth[b] (mcd)
MIS2-T1-Holocene	A, D	0.07–9.19	0.07–9.19
MIS6-T2-MIS5e	C	36.01–44.48	35.91–45.11

[a]mbsf = meters below seafloor.
[b]mcd = meters composite depth.

(hydrous hydrazine in a citric acid/ammonia buffer) was applied using boiling water bath sonication for several seconds every 2 min over a total duration of 30 min. Organic matter was removed using 100 μL of hydrogen peroxide (H_2O_2 30%) and 10 mL de NaOH 0.1 M, for 10 min in a 70°C in a bath, sonicating samples, every 2 and 5 min. Weak acid (0.001 M HNO_3) leaching was used as a final cleaning step to remove adsorbed contaminants before dissolving the foraminiferal calcite in 400 μL of 1% HNO_3. Preliminary calcium [Ca^{2+}] determination was provided by analyzing an aliquot of the samples (20 μL in 980 μL ultrapure 1% HNO_3) using an Agilent model 7500ce Inductively Coupled Plasma Mass Spectrometer. The remaining solutions were diluted to 40 ppm [Ca^{2+}] and injected into the inductively coupled plasma–mass spectrometry. Aluminum [Al^{3+}], manganese [Mn^{2+}], and iron [Fe^{3+}] were also measured [*de Villiers et al.*, 2002; *Yu et al.*, 2005] as indicators of possible silicate and clay mineral contamination and Fe-Mn oxide coatings [*Boyle*, 1983; *Barker et al.*, 2003; *Pena et al.*, 2005]. Analytical precision was monitored calculating the relative standard deviation (RSD) of two in-house standard solutions, CS2 (Mg/Ca = 2.571 ± 0.003) and CS4 (Mg/Ca = 7.713 ± 0.009 mmol mol^{-1}) analyzed every 5 and 10 samples, respectively, with an average RSD of 1.69% (n = 65). A limestone standard (ECRM752-1) with a specified Mg/Ca of 3.75 mmol mol^{-1} was measured [*Greaves et al.*, 2008] yielding 3.77 ± 0.09 mmol mol^{-1}. In order to identify potentially contaminated samples we checked for covariation between Al/Ca, Fe/Ca, Mn/Ca, and Mg/Ca ratios [*Barker et al.*, 2003; *Ferguson et al.*, 2008; *Pena et al.*, 2005] but no correlation was found between them (Al/Ca versus Mg/Ca, r^2 = 0.01; Mn/Ca versus Mg/Ca, r^2 = 0.03; Fe/Ca versus Mg/Ca, r^2 = 0.04). Using absolute Al/Ca and Mn/Ca ratios as a further contamination test [*Boyle*, 1983; *Wit et al.*, 2010] we rejected all samples that yielded Al/Ca ratios >400 μmol/mol and/or Mn/Ca ratios >100 μmol/mol. Fe/Mg ratios were used as another nominal control for silicate contamination [*Barker et al.*, 2003]. Fe/Mg ratios were high overall at ODP976 and we rejected 47 samples that displayed parallel increases in Fe/Mg and Mg/Ca or yielded exceptionally high Fe/Mg ratios.

2.5. Mg/Ca Temperature Estimation

Mg/Ca ratios were converted into temperature estimates using the *Elderfield and Ganssen* [2000] calibration for *G. bulloides*. Propagating the analytical error (± 0.05°C), calibration error (± 1.1°C) [*Elderfield and Ganssen*, 2000], cleaning procedure error (± 0.2°C) [*Barker et al.*, 2003], and natural variability error (± 0.4°C) [*Barker et al.*, 2003] yielded an overall error of the temperature estimate of 1.2°C. The resulting Mg/Ca temperature profiles were highly variable, displaying frequent single-point excursions that exceeded the propagated error (supporting information). The core-top Mg/Ca temperature estimate in our data set of 17.6°C matches observed spring surface temperatures in the region of 17–18°C that are shown in the MEDATILAS II and World Ocean Atlas WOA09 [MEDARGroup/MEDATLAS database, 2002, http://www.ifremer.fr/medar/cdrom_database.htm.); *Antonov et al.*, 2010; *Locarnini et al.*, 2010]. Satellite observations from the Aqua Moderate Resolution Imaging Spectroradiometer NASA database (http://modis.gsfc.nasa.gov) also give Alboran Sea spring surface temperatures of 17.5°C. Core-top Mg/Ca ratios from sites Alb-1 and T-1, both nearby ODP976 (Figure 1), yielded temperatures of 17.4°C and 18.1°C [*Masqué et al.,* 2003; I. Cacho, personal communication, 2013]. In addition, the shell flux of *G. bulloides* that was used in this study for Mg/Ca analysis occurs in spring [*Bárcena et al.*, 2004; *Hernández-Almeida et al.*, 2011; *Rigual-Hernández et al.*, 2012] which further corroborates the match of the ODP976 core-top Mg/Ca temperature estimate with observed spring temperatures. Hence, our core-top temperature estimate matches observed and reconstructed temperatures at and near the core location confirming the application of the Mg/Ca calibration.

Paleotemperature studies in the Alboran Sea [*Cacho*, 1999; *Martrat et al.*, 2004] report maximum SST during MIS5e of 23°C, corresponding to Mg/Ca ratios in the range of 6 mmol mol^{-1}. Hence, we considered temperatures of 23°C an upper threshold for ODP976. After cleaning out all Mg/Ca data that coincided with elevated Al/Ca, Mn/Ca, and anomalously high Fe/Mg levels the Mg/Ca temperatures along the down-core profiles in several cases reached above this threshold, up to 26°C. In order to eliminate these elevated temperatures from the record, a 5 point weighted average was computed and all temperature estimates exceeding the average by equal or more than 2 times the propagated temperature error were eliminated (supporting information). This final data reduction did not alter the fine structure and amplitude of the Mg/Ca temperature profile.

Salinity has been indicated as a potential temperature-independent control on Mg/Ca ratios in foraminiferal calcite [*Ferguson et al.*, 2008; *Arbuszewski et al.*, 2010], but we rule out such an influence as a major contributor to the down-core Mg/Ca variability. First, we note that ODP976 is in the Atlantic inflow where salinities are

low compared to the high-salinity settings where salinity significantly impacts Mg/Ca ratios in biogenic carbonate [e.g., *Ferguson et al.*, 2008; *Hoogakker et al.*, 2009]. Second, coupled ocean atmosphere circulation modeling by *Liu et al.* [2009] simulated a salinity increase of 2 psu at the Iberian margin in response to the termination of the Heinrich meltwater event H1 freshwater forcing. Using a Mg/Ca sensitivity of 4–11% per unit salinity increase [*Nürnberg et al.*, 1996; *Lea et al.*, 1999], we estimate a salinity-induced effect on Mg/Ca temperatures of no more than 1°C which compares to a Mg/Ca temperature range of 6°C along the ODP976 down-core profiles. This maximum amplitude is recorded during the Bølling/Allerød (B/A) and after H11 and is consistent with a modeled post-H-event temperature increase at the western Iberian Margin of 5–6°C [*Liu et al.*, 2009]. Much higher sensitivities are known to exist [*Ferguson et al.*, 2008], but these were connected with the strong salinity gradients in the Eastern Mediterranean where enhanced evaporation lower considerably the freshwater budget. Those settings are an unlikely reference for the ODP976 in the Alboran Sea.

2.6. Seawater δ^{18}O Calculation

We used *G. bulloides* δ^{18}O and Mg/Ca temperature estimates to compute the local seawater δ^{18}O ($\delta^{18}O_{sw}$) as an indication for salinity variations. First, we converted the composite relative sea level (RSL) record derived from corals [*Peltier and Fairbanks*, 2006; *Arz et al.*, 2007; *Bard et al.*, 2010] and the Red Sea hydraulic model [*Siddall et al.*, 2003; *Grant et al.*, 2012] into a profile of mean ocean δ^{18}O by applying a conversion of 0.008‰ per meter RSL [*Schrag et al.*, 1996]. This ice volume-corrected δ^{18}O ($\delta^{18}O_{ivc}$) was then inserted with Mg/Ca temperature into the *Bemis et al.* [2002] isotope paleotemperature equation to derive $\delta^{18}O_{sw}$. A $\delta^{18}O_{sw}$ of 1.0‰ was calculated from the ODP976 core-top $\delta^{18}O_{ivc}$ of 0.5‰ and Mg/Ca temperature of 17.6°C which matches the average value of 1.1 ± 0.2‰ VSMOW that was calculated from 20 in situ $\delta^{18}O_{sw}$ measurements of the upper 100 m water column in the Alboran Sea [*Pierre*, 1999].

2.7. Age Model

2.7.1. MIS2-T1-Holocene

The age model of the upper 15.9 mcd of the ODP976 sediment sequence was based on 13 accelerator mass spectrometry radiocarbon data published previously by *Combourieu-Nebout et al.* [2002]. The data were measured on monospecific *Globigerina bulloides* and *Neogloboquadrina pachyderma* (sin.) samples of the size fraction >125 μm. The initial age model of *Combourieu-Nebout et al.* [2002] was updated by using the recent Intcal13 calibration [*Reimer et al.*, 2013] to derive a calendar year timescale. A reservoir correction of 400 year was applied throughout except for the section between 15 and17 kyr for which higher reservoir ages of 800 years were found elsewhere in the Mediterranean [*Siani et al.*, 2001]. The age model yielded sedimentation rates between 15 and 40 cm kyr^{-1} (supporting information).

2.7.2. MIS6-T2-MIS5e

To establish the age model for the lower ODP976 sequence, we chose two iterative steps that exploited the tight correlation between North Atlantic and Mediterranean paleotemperature records and radiometrically dated speleothem records from Europe and Asia (Figure 2). Several studies indicated that the large-scale cooling of the North Atlantic region during periods of major freshwater perturbation caused altered atmospheric pressure gradients to intercept the direct solar forcing of the Asian monsoons thus phase-locking North Atlantic paleotemperature profiles with δ^{18}O records of Chinese speleothems [*Cheng et al.*, 2006; *Kelly et al.*, 2006; *Wang et al.*, 2001, 2005]. Paleomonsoon modeling of *Pausata et al.* [2011] added the constraint of temperature-driven isotope fractionation in conjunction with changes of North Indian surface-ocean climatology as a further constraint. Their model output shows increases in δ^{18}O of precipitation over India and of the water vapor arriving in East Asia during North Atlantic cold phases in response to cooling of the northern Indian Ocean. This complements the controls on Chinese speleothem δ^{18}O signals but does not change the temporal connection between speleothem δ^{18}O changes and North Atlantic climate; hence, it does not affect the synchronization of the ODP976 Mg/Ca temperature profile with the Chinese speleothem δ^{18}O record. Atmospheric CH_4 likewise was impacted by monsoon strength variations [*Blunier et al.*, 1998; *Masson-Delmotte et al.*, 2004] and the coeval changes that were observed between atmospheric CH_4, Mediterranean SST, and speleothem δ^{18}O provide extra support for the concept that Mediterranean (and North Atlantic) paleoclimatology and atmospheric CH_4 changes were directly connected with Asian monsoon variability [*Kelly et al.*, 2006; *Sánchez-Goñi et al.*, 2008].

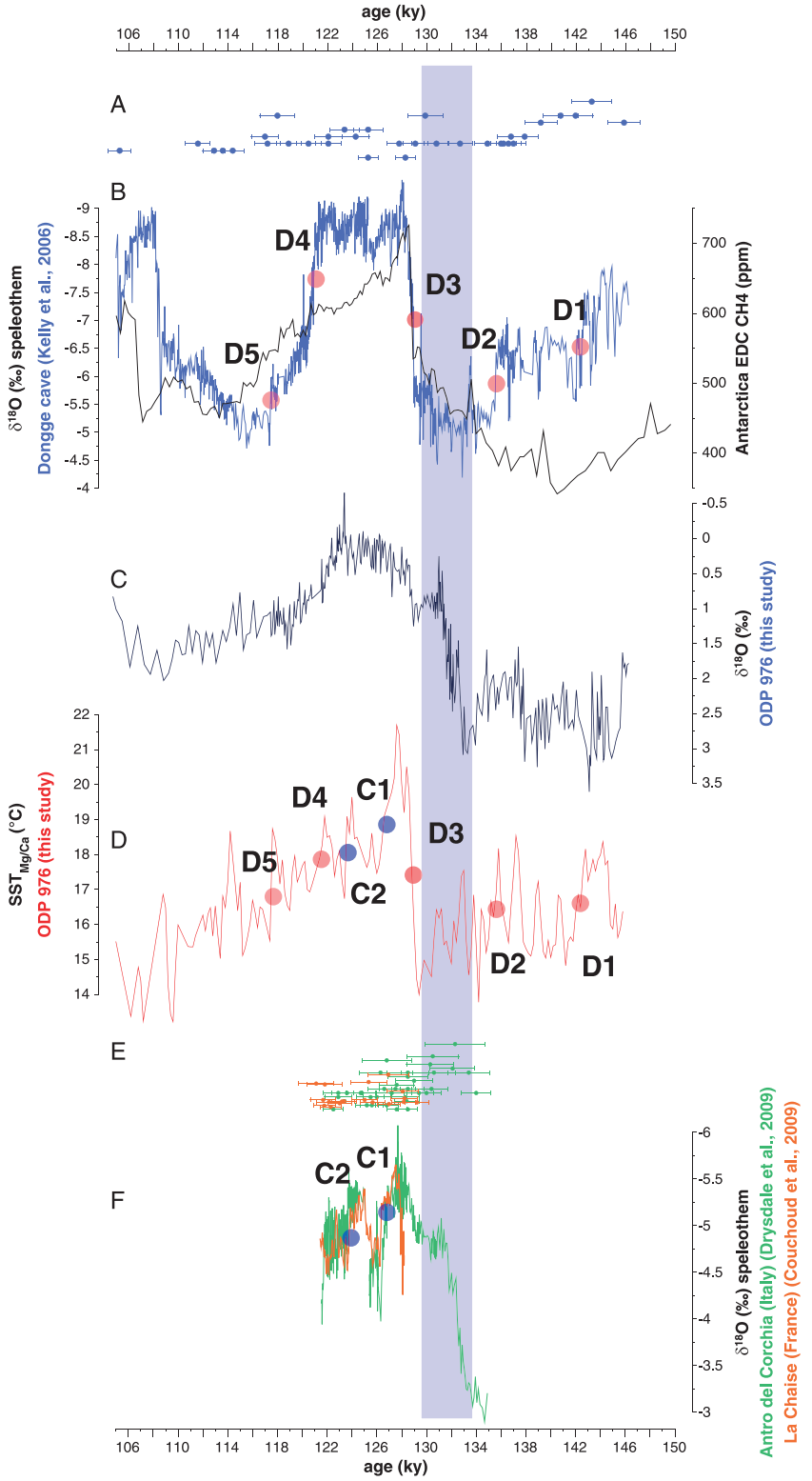

Figure 2. Synchronizing the ODP976 MIS6-T2-MIS5e sequence with speleothem $\delta^{18}O$ profiles from China and Mediterranean Europe. (a) Dongge Cave speleothem radiometric ages with 95% error bars [*Kelly et al.*, 2006]. (b) Dongge speleothem $\delta^{18}O$ profile (blue [*Kelly et al.*, 2006]) and Antarctic atmospheric CH4 record (black [*Loulergue et al.*, 2008]). (c) ODP 976 planktic $\delta^{18}O$ (*G. bulloides*). (d) ODP 976 Mg/Ca temperature record. (e) Radiometric ages with 95% error bars for the Antro del Corchia (AdC, green) and La Chaise de Vouthon (LCV, orange) speleothems [*Drysdale et al.*, 2009; *Couchoud et al.*, 2009]. (f) Speleothem $\delta^{18}O$ profiles of AdC (green) [*Drysdale et al.*, 2009] and LCV (orange) [*Couchoud et al.*, 2009]. Red dots and labels D1–D5 mark tie points used for synchronization with Dongge record. Blue dots and labels C1 and C2 mark tie points used for synchronization with AdC and LCV. Markers are listed in Table 2.

Table 2. Synchronization of ODP 976 SST and Speleothem δ^{18}O Profiles From Dongge Cave [*Kelly et al.*, 2006] and Antro del Corchia Cave [*Drysdale et al.*, 2009]

ODP976, Depth (mcd)	Speleothem Reference and Tie Points in Figure 2	Speleothem ^{230}Th Ages (Interpolated) (kyr)
36.88	Dongge Cave [*Kelly et al.*, 2006], D5	117.43
37.80	Dongge Cave [*Kelly et al.*, 2006], D4	121.43
38.92	Corchia Cave [*Drysdale et al.*, 2009], C2	123.66
39.78	Corchia Cave [*Drysdale et al.*, 2009], C1	126.54
40.25	Dongge Cave [*Kelly et al.*, 2006], D3	128.73
42.61	Dongge Cave [*Kelly et al.*, 2006], D2	135.57
44.14	Dongge Cave [*Kelly et al.*, 2006], D1	142.09

We chose the Dongge cave δ^{18}O record of *Kelly et al.* [2006] over similar records from the Hulu and Sanbao Caves [*Cheng et al.*, 2009; *Wang et al.*, 2001, 2008] because Dongge has a tighter age control with 26 ^{230}Th dates [*Kelly et al.*, 2006]. We tuned the ODP 976 Mg/Ca temperature record to the Dongge δ^{18}O record using a series of five tie points (Figure 2 and Table 2) connecting the midpoints of speleothem δ^{18}O and ODP976 temperature changes, including the most prominent events: the onset of the weak monsoon interval (WMI) at 135.6 kyr was linked with the first transition to lower Mg/Ca temperatures at ODP976; onset of Asian Monsoon strength at 128.7 kyr was connected with the abrupt temperature increase at ODP976 at the end of T2; and the end of the interglacial monsoon maximum at 121.4 kyr was connected with the mid-MIS5e temperature decrease at ODP976 (Figure 2). In a next step we correlated the MIS5e section of the ODP Mg/Ca temperature profile with the speleothem δ^{18}O records of Antro del Corchia (AdC) [*Drysdale et al.*, 2009] and La Chaise de Vouthon (LCV) [*Couchoud et al.*, 2009] caves in Italy and Southern France. The AdC and LCV speleothem δ^{18}O profiles are correlated structurally with SST and pollen profiles from the Iberian margin and with other speleothem δ^{18}O records from the eastern Mediterranean region demonstrating the sensitivity of both speleothems to changes of the North Atlantic paleoclimatology and ensuing moisture transports over the Mediterranean under variable air temperatures [*Drysdale et al.*, 2007; *Couchoud et al.*, 2009; *Drysdale et al.*, 2009]. We obtained two tie points for the ODP976 age model (Figure 2 and Table 2) by tuning the center points of the steep temperature decreases displayed at ODP976 during early MIS5e with the likewise steep δ^{18}O decreases at 123.7 kyr and 126.5 kyr in the Antro del Corchia and La Chaise records [*Couchoud et al.*, 2009; *Drysdale et al.*, 2009]. The structure of the Mg/Ca temperature profile on the resulting spelothem-based age model matches that of the Antarctic CH_4 profile, hence supporting the age modeling. The speleothem-synchronized age model yielded sedimentation rates between 30 and 45 cm kyr^{-1}. This age model updates the orbitally tuned age model of *Martrat et al.* [2014] and yields an optimized stratigraphic fit with the *Lisiecki and Raymo* [2004] age model (supporting information).

We assessed the viability of using radiometrically dated Chinese speleothem δ^{18}O profiles as a reference for ODP976 age modeling by graphically tuning the ODP976 Mg/Ca temperature profile of the MIS2-T1-Holocene section to the Hulu-Sanboa speleothem δ^{18}O profile of *Wang et al.* [2001, 2008] and then comparing the tuned age scale to the ^{14}C-based age model of this section (supporting information). Applying a minimum of six tie points at the base of the record, the onset and end of the B/A and YD, the early Holocene climatic optimum and at the core top yielded a good structural fit between the speleothem and ODP976 profiles. This age model was transferred to the ODP976 δ^{18}O profile which yielded an excellent fit with the speleothem δ^{18}O record. Offsets between the speleothem-tuned and ^{14}C-based age models are between 500 and 900 years during T1, while the offsets in the Holocene of 300 years and in MIS2 of 40 years are not representative. The structure of the ODP976 Mg/Ca profile did not allow to define extra tie points beyond the ones in the early Holocene and the core top and between the start of the B/A and base of the section. The age offsets during T1 are constrained by four graphical tie points and six calibrated ^{14}C-based age datums and are an order larger than the analytical error of 50–90 years of the radiocarbon ages in this core section. The larger age offsets between the two age models during T1 encompass the B/A and Y/D period which are known for changes in atmospheric and oceanic radiocarbon inventories stemming from the emission of old carbon from the ocean during major ocean overturning changes at that time [*Stuiver and Braziunas,* 1993; *Bard et al.,* 2004; *Hughen et al.,* 2006]. But these factors are embedded in the radiocarbon calibration and are not likely a source

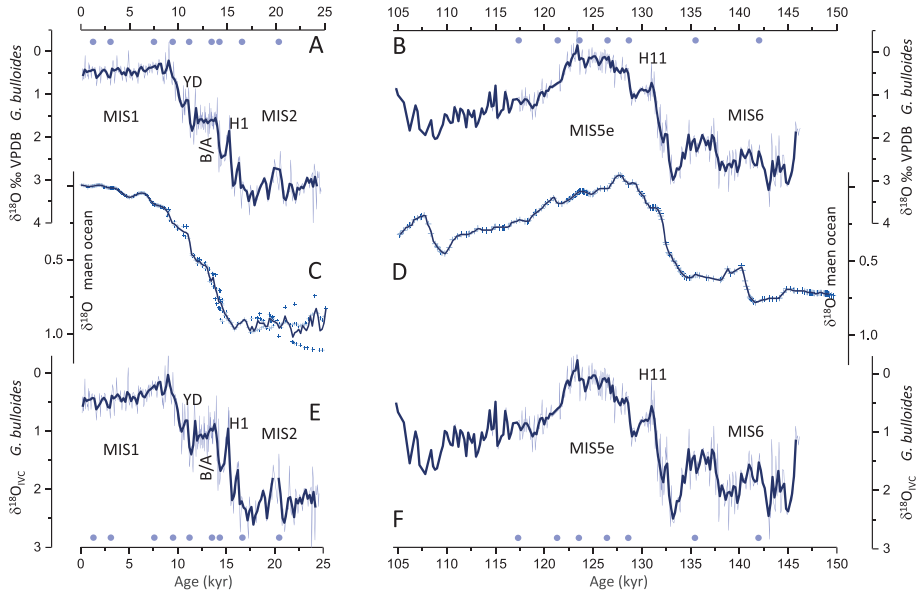

Figure 3. *G. bulloides* $\delta^{18}O$ profiles of ODP976 and ice volume correction. (a) $\delta^{18}O$ profile of the MIS2-T1-Holocene sequence and (b) of the MIS6-T2-MIS5e sequence. (c) Mean ocean $\delta^{18}O$ profile of the MIS2-T1-Holocene sequence and (d) of the MIS6-T2-MIS5e sequence. (e) Ice volume-corrected $\delta^{18}O_{ivc}$ of the MIS2-T1-Holocene sequence and (f) of the MIS6-T2-MIS5e sequence. Mean ocean $\delta^{18}O$ profiles were calculated from global relative sea level profiles (see text). Dots along the top *x* axis in Figure 3a mark position of calibrated radiocarbon datums and in Figure 3b tie points used for synchronization with speleothem $\delta^{18}O$ records (see Figure 2 and Table 2).

for the age offsets. Moreover, the Intcal13 age model yielded younger ages than the speleothem-tuned model; hence, surface water reservoir age variations can be excluded as a source for the offsets. Taking the maximum calculated age offsets during T1 at face value, we consider a conservative age model uncertainty of better than 1 kyr.

3. Results

3.1. Planktic $\delta^{18}O$ Profiles

Planktic $\delta^{18}O$ along the MIS2-T1-Holocene and MIS6-T2-MIS5e sequences display T1 and T2 as multiple-step transitions with glacial-interglacial amplitudes of 2.8‰ and 2.3‰, respectively (Figures 3a and 3b). Mean glacial values during MIS2 (3.15 ± 0.32‰, $n = 78$) are heavier than those of MIS6 (2.45 ± 0.46‰, $n = 104$) and mean MIS5e values (0.13 ± 0.24‰, $n = 37$) are lighter than early Holocene values (0.38 ± 0.25‰, $n = 19$). Comparison with the mean ocean $\delta^{18}O$ profile that was derived from the global sea level record (see section 2.6) shows that glacial-interglacial $\delta^{18}O$ amplitudes along the *G. bulloides* $\delta^{18}O$ profiles exceed the mean ocean $\delta^{18}O$ shifts during T1 and T2 by 1.6–1.9‰. Subtracting the mean ocean $\delta^{18}O$ from the ODP976 planktic $\delta^{18}O$ yielded the local ice volume-corrected $\delta^{18}O$ profile ($\delta^{18}O_{ivc}$) which maintained the fine structure of the original *G. bulloides* $\delta^{18}O$ profile and reflects variations of the local temperature and salinity fields at the core site (Figures 3e and 3f).

The T1 structure of the $\delta^{18}O_{ivc}$ profile mimics the classical sequence of events (Figure 3e) including Heinrich event H1 that is displayed at ODP976 with two negative $\delta^{18}O_{ivc}$ peaks mimicking the incursion of meltwater from ice sheet collapse; the Bølling/Allerød (B/A) marking the end of the H1 freshwater perturbation and signaling the kick starting of the Atlantic Meridonal Overturning Circulation (AMOC) [*Weaver et al.*, 2003; *Gherardi et al.*, 2009]; the Younger Dryas (YD) cold spell that is indicated by a transient increase of $\delta^{18}O_{ivc}$ values; and the subsequent transition into the Holocene with a brief positive $\delta^{18}O_{ivc}$ excursion mimicking the 8.2 kyr cold episode [*Rohling and Pälike*, 2005; *Cheng et al.*, 2009].

The structure of T2 is most prominently shaped by the negative $\delta^{18}O_{ivc}$ "hump" associated with H11 (Figure 3f). The transient negative "precursor" peak centered at 132.5 kyr resembles in amplitude and

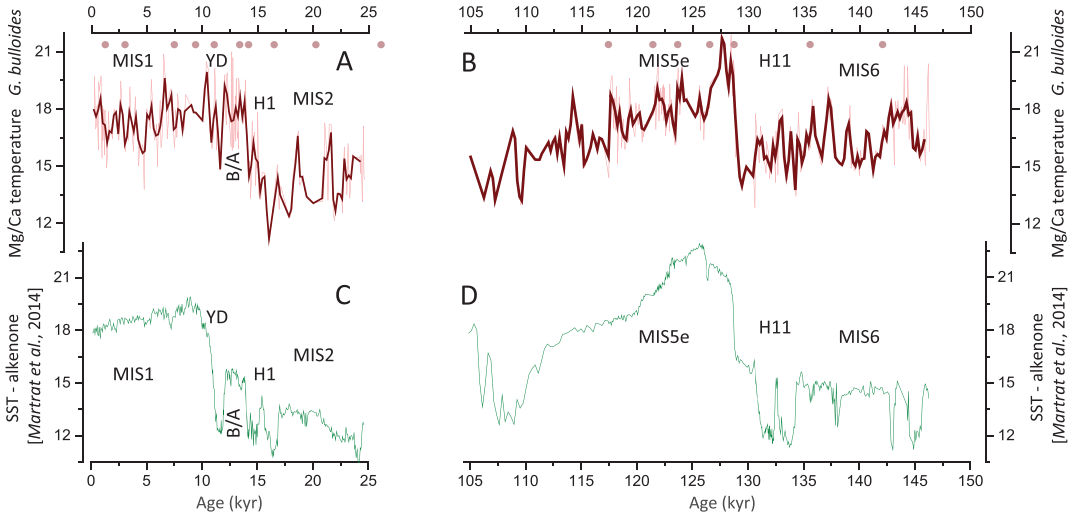

Figure 4. Paleotemperature records at ODP976. *G. bulloides* Mg/Ca temperature profile (a) of the MIS2-T1-Holocene sequence and (b) of the MIS6-T2-MIS5e sequence. Thick lines are a 200 year step Gaussian smooth with a 600 year wide window. Alkenone temperature profile (c) of the MIS2-T1-Holocene sequence and (d) of the MIS6-T2-MIS5e sequence [*Martrat et al.*, 2014].

absolute $\delta^{18}O_{ivc}$ values the first of two $\delta^{18}O_{ivc}$ peaks associated with H1 during T1. In contrast to H1 the H11 anomaly is displayed as an uninterrupted $\delta^{18}O_{ivc}$ minimum lasting about 30% longer than the $\delta^{18}O_{ivc}$ minimum of H1.

3.2. Mg/Ca Temperatures

The Mg/Ca temperature records display disparate structures during both stratigraphic sequences (Figures 4a and 4b). Temperatures during MIS2 (14.6 ± 1.5°C, $n = 72$) are about 2°C lower than during MIS6 (16.4 ± 0.95°C, $n = 133$), while MIS5e (18.2 ± 1.4°C, $n = 100$) is slightly warmer than the early Holocene (17.5 ± 0.9°C, $n = 10$). An outstanding feature is the transient warm overshoot to 20.2 + 1.2°C ($n = 13$) during early MIS5e which is about 3°C warmer than the early Holocene climatic optimum. In line with the multistep transition seen in the $\delta^{18}O$ profiles, T1 displays several temperature excursions coinciding with H1 (12.9 ± 1.7°C, $n = 4$), the Bølling/Allerød (18.8 ± 2.1°C, $n = 35$), and the YD cold episode (minimum $T = 15.9°C \pm 0.6°C$, $n = 6$). Additional features of the Mg/Ca temperature profiles are the B/A reaching full interglacial temperature levels which is warmer than documented at open-ocean settings in the North Atlantic, and the YD and H1 are recorded with early cold phases followed by warmer phases. T2 does not display alternating cold-warm anomalies but is dominated by the temperature minimum of H11 that ends with a single-step abrupt warming by 6°C from glacial level temperatures to the warm overshoot of early MIS5e. Hence, while the $\delta^{18}O_{ivc}$ records during T1 and T2 display multiple steps and exhibit salient midtermination minima, the Mg/Ca temperature profiles reveal significant differences.

3.3. Mg/Ca Temperatures Versus Alkenone-based SST

Martrat et al. [2014] recently published an alkenone-based SST profile from ODP976 that is different in structure from our Mg/Ca temperature record (Figures 4c and 4d). The most notable differences are the overall higher variability and lower temperature increases during the glacial terminations seen in the Mg/Ca temperature reconstruction, and the low interglacial variability of the alkenone SST that remains below the uncertainty of this method (0.5°C) [*Martrat et al.*, 2014]. The offset between Mg/Ca- and alkenone-derived temperatures reverses along the records with alkenone SST dropping below Mg/Ca temperatures during glacials (MIS6 and 2) and increasing above Mg/Ca temperatures during interglacials (MIS5e and 1). The amplitude of the Mg/Ca temperature increase during the B/A is about twice the coeval amplitude displayed by alkenone-derived SST with Mg/Ca temperatures reaching Holocene levels while alkenone SST reach values halfway between MIS2 and Holocene levels. The early MIS5e Mg/Ca temperature overshoot coincides in the alkenone SST profile with a first post-H11 warming step, while the MIS5e SST maximum in the alkenone record is reached 1 kyr after the Mg/Ca temperature maximum. Finally, Mg/Ca temperatures between 131 and 128 kyr B.P. display a minimum at the same time when

alkenone SST show a 4°C warming. This section coincides with the mid-T2 negative $\delta^{18}O_{ivc}$ anomaly that reflects the low-salinity meltwater environments of H11 (Figure 3f). Micropaleontologic inspection revealed maximum shows of *Bitectatodinium tepikiense* dinoflagellate cysts in this core interval (L. Londeix, personal communication, 2013) which is a marker species for cold-water environments and large seasonal temperature amplitudes [*Rochon et al.*, 1999; *Marret and Zonneveld*, 2003]. The coincidence of this species with the negative $\delta^{18}O_{ivc}$ anomaly fits with the incursion at ODP976 of cold and low-salinity waters of H11 that were advected to the Mediterranean via the Atlantic inflow [*Combourieu-Nebout et al.*, 2002, 2009; *Sierro et al.*, 2005] which is consistent with the negative Mg/Ca temperature anomaly.

Differences between Mg/Ca- and alkenone-derived temperature profiles were observed at Atlantic, Pacific, and Southern Oceans core sites and were interpreted to reflect combined changes of phytoplankton and zooplankton ecological behavior with consequences for proxy formation and temperature recording [*Leduc et al.*, 2010]. Seasonal changes and variable depth habitats can leave their imprints on the Mg/Ca temperature reconstructions if *G. bulloides* records springtime temperatures [*Elderfield and Ganssen*, 2000; *Ganssen and Kroon*, 2000] at subsurface depths [*Mortyn and Charles*, 2003; *Jonkers et al.*, 2013], while alkenones record annually integrated temperatures at the sea surface [*Martrat et al.*, 2007; *Huguet et al.*, 2011; *Dos Santos et al.*, 2013]. However, such an interpretation remains open for debate because a recent temperature calibration at the Iberian Margin suggested that the maximum production of alkenone-producing haptophyte algae takes place during the winter season [*Rodrigues et al.*, 2012]. If paleoecology indeed played a role at ODP976 in causing the offset Mg/Ca and alkenone temperature reconstructions such an influence must have changed systematically between glacial and interglacial conditions in order to reverse the offset between alkenone and Mg/Ca temperatures from negative during glacials to positive during interglacials.

In a recent model-data comparison *Laepple and Huybers* [2013, 2014] estimated that measurement noise, bioturbation, and frequency aliasing cause Mg/Ca temperature reconstructions to systematically average more than twice the variance of alkenone temperature records. We can exclude sampling statistics and aliasing as a source because the alkenone and Mg/Ca-based reconstructions are at the same site. It needs to be noted that Mg/Ca was measured on only 50% (MIS2-T1-Holocene) and 65% (MIS6-T2-MIS5e) of all samples used for alkenone analysis, but whenever Mg/Ca and alkenone were analyzed in pairs they were measured on aliquots of the same samples.

This leaves the possibility that the differences between the alkenone and Mg/Ca temperature profiles originate from the fact that alkenones as molecular components are several orders of magnitude more abundant in sediment samples and potentially represent a larger number of years than the far smaller number of foraminiferal shells from which the Mg/Ca temperatures were derived [*Laepple and Huybers*, 2013, 2014]. It can be expected therefore that foraminiferal Mg/Ca temperature reconstructions are more sensitive to seasonal and interannual variabilities while the large number of alkenone molecules reduces these influences by up to 50% [*Laepple and Huybers*, 2013]. Lateral transport of alkenones and postmortem shells of planktic foraminifera by ocean currents has been indicated as a potential complication in alkenone and foraminiferal-based temperature reconstructions [*Gyldenfeldt et al.*, 2000; *Sicre et al.*, 2005; *van Sebille et al.*, 2015] but at this stage we cannot quantify a possible differential impact of lateral transportation by the Atlantic inflow on both temperature reconstructions. Neither is it obvious why this would cause the gradient between both reconstructions to reverse. But we note that a *G. bulloides* Mg/Ca profile from the western Iberian margin [*Skinner et al.*, 2003] displays B/A warming of a similar amplitude to that at ODP976 and that this high-amplitude warming is consistent with the magnitude of post-Heinrich event warming at this location that was simulated with numerical modeling [*Liu et al.*, 2009]. This lends credence to the ODP976 Mg/Ca temperature profile as representing the regional paleotemperature history. The differences between the Mg/Ca and alkenone records either reflect temperature seasonality or are a function of the depth habitats of *G. bulloides* as the Mg/Ca signal carrier and haphtophyte algae as alkenone producers. We employ the Mg/Ca temperature estimates together with $\delta^{18}O_{ivc}$ to estimate seawater $\delta^{18}O$ as an indicator of surface layer salinity variation.

4. Discussion

Marine and terrestrial records provided ample evidence for past climate variability in Mediterranean Europe on orbital and suborbital timescales. Paleoceanographic profiles at Mediterranean Sea core sites displayed a

close structural correlation with paleoclimatic variability recorded in North Atlantic marine cores and Greenland ice cores [e.g., *Cacho et al.*, 2001; *Sbaffi et al.*, 2001; *Marchal et al.*, 2002; *Rohling et al.*, 2002; *Sprovieri et al.*, 2003; *Martrat et al.*, 2004; *Pérez-Folgado et al.*, 2004; *Moreno et al.*, 2005] which demonstrated the impact of the North Atlantic paleoclimatology on Mediterranean Sea circulation and climate variability. Some of the variability was connected with changes of the Mediterranean's marine heat and freshwater budget which was diagnostic of atmospheric circulation changes. Frequent intrusions of northerly polar and southerly tropical air masses were indicated in response to latitudinal migrations of the polar front to the north and the Intertropical Convergence Zone further south [e.g., *Cacho et al.*, 1999; *Rohling et al.*, 2002; *Kuhlemann et al.*, 2008; *Rodrigo-Gámiz et al.*, 2011; *Sprovieri et al.*, 2012]. This impacted the temperature and moisture gradients across the Mediterranean with consequences for the water exchange between the Mediterranean and the North Atlantic [*Cacho et al.*, 2000; *Rogerson et al.*, 2010; *Rodrigo-Gámiz et al.*, 2011]. The combined influence of these changes impacted the Mediterranean marine system in its entirety including perturbations of the vertical stratification and trophic levels, ecosystems, and the thermohaline circulation at large [*Sierro et al.*, 2005; *Incarbona et al.*, 2011; *Sprovieri et al.*, 2012; *Di Stefano et al.*, 2014, 2015]. Comparison with pollen sequences [*Gasse and Van Campo*, 1994; *deMenocal and Baker*, 2000; *Combourieu-Nebout et al.*, 2002; *Sánchez-Goñi et al.*, 2002; *Combourieu-Nebout et al.*, 2009; *Incarbona et al.*, 2010] and speleothem profiles [*Allen and Huntley*, 2009; *McDermott*, 2004; *Genty et al.*, 2006; *Drysdale et al.*, 2007; *Zanchetta et al.*, 2007; *Couchoud et al.*, 2009; *Moreno et al.*, 2010] made a strong case of a tight coupling of Mediterranean marine paleoclimatology and terrestrial climate variability over the surrounding borderlands. These studies demonstrated that the Mediterranean is a perfect site to trace the paleoclimatology of the North Atlantic region and the Northern Hemisphere at large.

With our ODP976 records we expand on this work and shift the focus from the last glacial-interglacial cycle to the transition from the penultimate glacial (MIS6) to the last interglacial MIS5e. First, we use the MIS2-T1-Holocene sections to test the suitability of the ODP976 paleoprofiles to depict the North Atlantic paleoclimatology.

4.1. The MIS2-T1-Holocene Sequence

The ODP976 planktic $\delta^{18}O$ and Mg/Ca temperature profiles resolve this period at a multidecadal temporal resolution and display the classical sequence of events that is exemplified in the Greenland ice core $\delta^{18}O$ profile (Figures 5a–5c). The early-deglacial H1 event that was linked with the large-scale destabilization of the circum-North Atlantic ice sheets [*Heinrich*, 1988; *Hemming*, 2004] is seen in the ODP976 records as a prominent cold episode with two negative peaks in the *G. bulloides* $\delta^{18}O$ record. The local $\delta^{18}O_{sw}$ profile that was calculated from *G.bulloides* $\delta^{18}O$ and Mg/Ca temperatures using the *Bemis et al.* [2002] equation displays a negative anomaly during H1 of 1‰ (Figure 5d) signifying the incursion of ^{18}O depleted meltwaters and low seawater salinity. A similar magnitude $\delta^{18}O_{sw}$ anomaly was reconstructed at the Iberian margin [*Skinner et al.*, 2003] implying that the H1 isotope anomaly was quantitatively advected with the meltwater to ODP976.

The mid-T1 Bølling/Allerød (B/A) warming at the end of H1 was captured in other paleorecords from the region and linked with increased marine heat transports to the North Atlantic [*Ruddiman and McIntyre*, 1981; *Cacho et al.*, 1999; *Shackleton et al.*, 2000; *Eynaud et al.*, 2009; *Naughton et al.*, 2009; *Liu et al.*, 2009; *Voelker and de Abreu*, 2011]. ODP976 Mg/Ca temperatures reached full interglacial levels at that time. A similar high-amplitude warming is reproduced in a *G. bulloides* Mg/Ca temperature record from the western Iberian margin [*Skinner et al.*, 2003] (Figure 5e). This warming reflected the heat transport in the North Atlantic subtropical gyre whose eastern boundary current extended to the Iberian margin deflecting some of its warm waters to the Alboran Sea by way of the Atlantic-to-Mediterranean surface water flow. It mimics the sharp temperature increase in the region that was simulated with coupled atmosphere-ocean general circulation modeling in response to the abrupt AMOC strengthening after the termination of the H1 freshwater perturbation [*Liu et al.*, 2009]. The subsequent Younger Dryas (YD) cold spell was linked with renewed freshwater-induced weakening of the AMOC and the ensuing reduction of the poleward heat transport triggered a transient return to nearly full-glacial conditions around the North Atlantic [*Walker et al.*, 2009]. At ODP976 this period is recorded with an early phase of increased $\delta^{18}O$ and cold SST that was followed by a second phase of warmer SST and depleted $\delta^{18}O$. A two-phased structure of the YD is reproduced by fossil pollen assemblages at ODP976 that indicated an abrupt shift from semidesert to forest taxa reflecting a shift from cold arid to warm humid conditions [*Combourieu-Nebout et al.*, 2009]. A

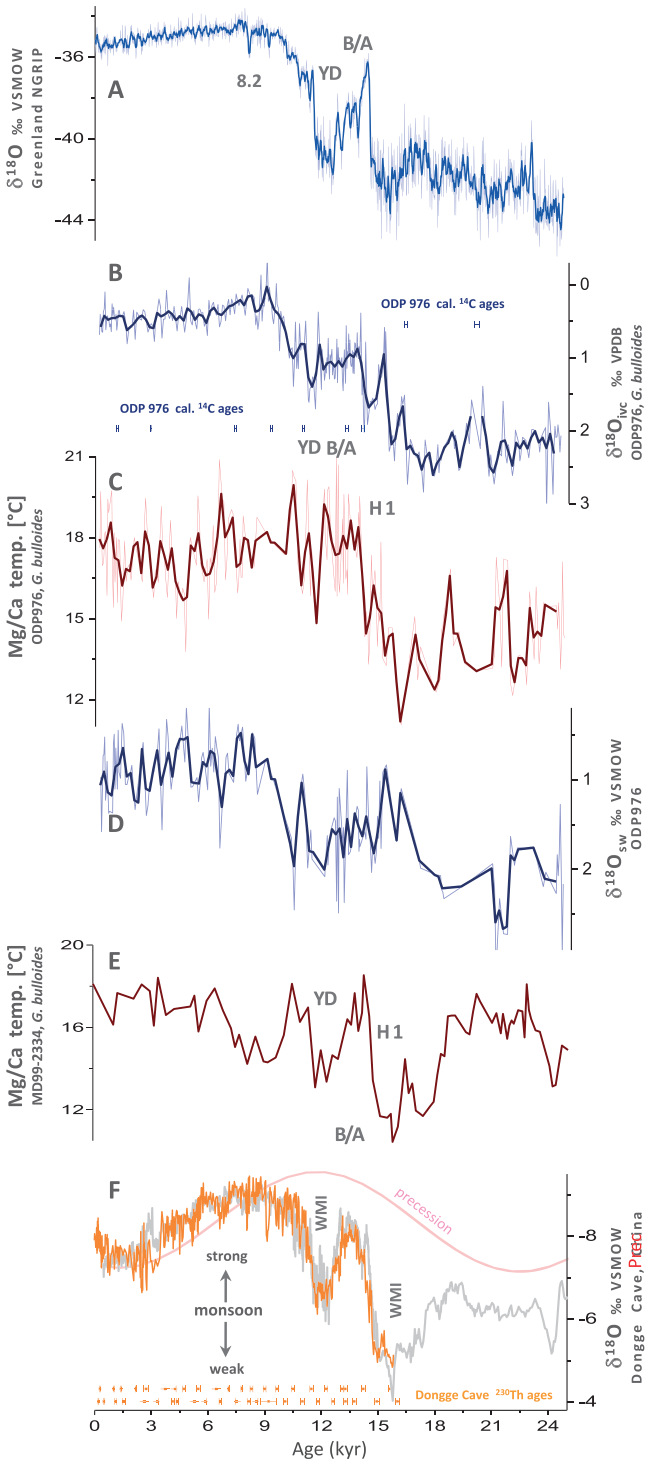

Figure 5. North Atlantic palaeoclimatology of the MIS2-T1-Holocene sequence. (a) Greenland NGRIP δ^{18}O record [*North Greenland Ice Core Project members*, 2004]. (b) ODP976 *G. bulloides* δ18O$_{ivc}$ profile. Dots mark calibrated radiocarbon datums. (c) ODP976 *G. bulloides* Mg/Ca temperature profile. (d) ODP976 δ18O$_{sw}$ profile calculated from δ^{18}O$_{ivc}$ and Mg/Ca temperatures shown in Figures 5b and 5c. (e) *G. bulloides* Mg/Ca temperature profile of core MD99-2331 from the western Iberian margin [*Skinner et al.*, 2003] using the age model of *Gouzy et al.* [2004] and *Sánchez-Goñi et al.* [2013]. (f) Speleothem δ^{18}O profile from Dongge Cave [*Dykoski et al.*, 2005]. Speleothem ^{230}Th datums are marked along bottom *X* axis. Red line is unlagged orbital precession highlighting deviation of monsoon strength from insolation forcing during weak monsoon intervals (WMI) of T1. H1 = Heinrich meltwater event 1, B/A = Bølling/Allerød warm phase, YD = Younger Dryas cold spell, and 8.2 = early Holocene cold snap at 8.2 kyr.

two-phased structure of the YD is also consistent with an early intra-YD Mediterranean warming observed in previous studies [*Goslar et al.*, 1993; *Brauer et al.*, 2000; *Cacho et al.*, 2000, 2002]. The final transition into the Holocene is depicted at ODP976 by a gradual decrease to interglacial $\delta^{18}O$ values. Mg/Ca temperatures already had reached interglacial levels during the B/A, while the YD resulted in an only modest temperature decrease. Therefore, the transition from the YD to the Holocene coincided with an only small increase of Mg/Ca temperatures by some 1.5°C.

The early Holocene cold episode at 8.2 kyr that is well marked in the Greenland profile and other records from the North Atlantic region and the wider Northern Hemisphere was attributed to a transient AMOC slowdown in conjunction with a terminal meltwater outflow to the North Atlantic [*Rohling and Pälike*, 2005; *Cheng et al.*, 2009; *Ellison et al.*, 2006; *Pross et al.*, 2009; *Dixit et al.*, 2014]. The 8.2 kyr event in the subpolar North Atlantic was associated with two cooling events dated to 8.5 and 8.3 kyr [*Ellison et al.*, 2006] and the ODP976 Mg/Ca temperature profile indeed shows two transient cold excursions in the early Holocene section. They are framed by two calibrated ^{14}C age datums of $9.4 \pm .06$ kyr and $7.5 \pm .05$ kyr that yielded interpolated ages of 7.6 and 8.4 kyr for both transients. This does not allow for a more precise correlation with the 8.2 kyr event, but we note that both cold excursions at ODP976 were accompanied with low-$\delta^{18}O_{sw}$ indicating surface water freshening which is a known feature of the 8.2 kyr event [*Rohling and Pälike*, 2005; *Ellison et al.*, 2006].

Finally, the structure of the ODP976 Mg/Ca temperature profile fits with that of the Dongge Cave speleothem $\delta^{18}O$ record in that the temperature anomalies expressed during H1, B/A, and the YD coincide with $\delta^{18}O$ excursions in the speleothem profile that signify the alternation between collapsed and strengthened monsoons (Figure 5f) [*Cheng et al.*, 2006; *Kelly et al.*, 2006; *Wang et al.*, 2001, 2005; *Pausata et al.*, 2011]. We conclude that the ODP976 $\delta^{18}O$ and Mg/Ca temperature profiles provide a viable representation of the North Atlantic climatology. Temporal offsets between the ice core, marine, and speleothem records shown in Figure 5 remain within the estimated age model uncertainty of about 1 kyr.

4.2. The MIS6-T2-MIS5e Sequence

The ODP976 $\delta^{18}O_{ivc}$ profile of the MIS6-T2-MIS5e sequence displays the penultimate glacial-interglacial transition as a multistep transition that mimics features of T1 (Figure 6). These are the increase to maximum $\delta^{18}O$ values immediately before the onset of deglaciation, a steep multistep $\delta^{18}O$ decrease during the first half of the termination, and a midtermination $\delta^{18}O$ plateau that is followed by a transient $\delta^{18}O$ increase and a likewise steep final $\delta^{18}O$ decrease to interglacial levels. During T1 these isotope events involved an alternation between polar-cold and warm conditions of the H1-B/A-YD climatic oscillation. For T2 the ODP976 Mg/Ca profile (Figure 6c) suggests a different temperature pattern. The sudden multistep $\delta^{18}O$ decrease at the end of MIS6 and the mid-T2 $\delta^{18}O$ plateau coincided with cold Mg/Ca temperatures that dominated much of T2 and remained at the temperature level of MIS6. $\delta^{18}O_{sw}$ that was calculated from $\delta^{18}O_{ivc}$ and Mg/Ca temperature displays a pronounced negative anomaly diagnosing low salinity in this section (Figure 6d). Cold polar temperatures and low salinity are type characteristics of Heinrich events and their occurrence during T2 at ODP976 marks the advection of modified North Atlantic waters that were impacted by the H11 meltwater surge. Maximum abundance of the cold-water dinoflagellate *B. tepikiense* at ODP976 is further evidence of the subpolar conditions at this time (L. Londeix, personal communication). The fact that H11 was not associated with a major freshwater surge in Hudson Strait [*Obrochta et al.*, 2014] suggests that the $\delta^{18}O_{sw}$ anomaly at ODP976 was derived from the disintegrating Saalian ice sheet in Eurasia (see below).

The imprints of Heinrich events were traced across the Mediterranean and were suggested to be linked with the advection of subpolar low-salinity water from the North Atlantic and coincident polar air outbreaks over the Mediterranean [*Cacho*, 1999; *Rohling et al.*, 2002; *Cacho et al.*, 2006; *Frigola et al.*, 2008; *Rodrigo-Gámiz et al.*, 2011; *Sprovieri et al.*, 2012; *Di Stefano et al.*, 2015]. Comparison with the hydrographic imprint of H1 shows that the $\delta^{18}O_{sw}$ anomaly produced by H11 at ODP976 was about twice as high and lasted approximately 30% longer than H1. Ice-rafted debris maxima generated by H11 at North Atlantic ODP980 [*Oppo et al.*, 2006] incurred between 131 and 134.5 kyr (age scale of *Govin et al.* [2012]) and at the western Iberian margin site MD01-2444 [*Skinner and Shackleton*, 2006] between 129 and 135.4 kyr (age scale of *Hodell et al.* [2013]), coinciding with a negative $\delta^{18}O_{sw}$ anomaly at this site (Figure 6f). This timing

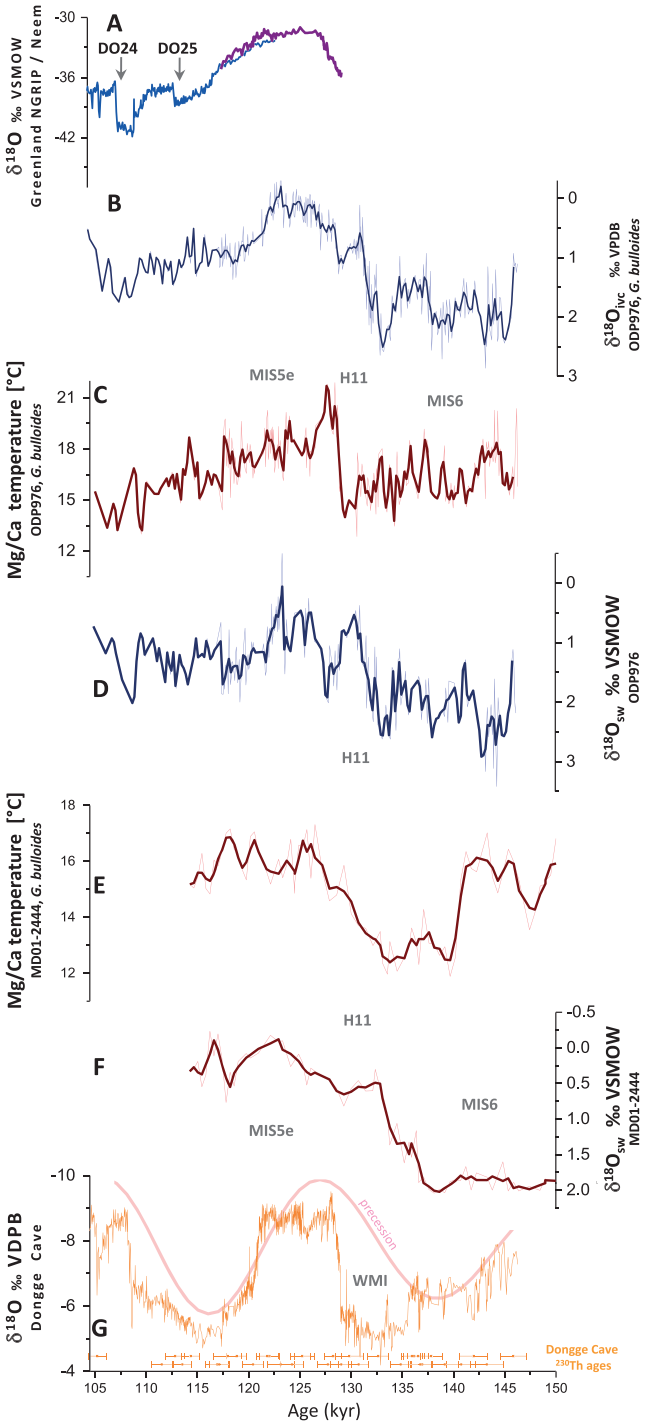

Figure 6. North Atlantic palaeoclimatology of the MIS6-T2-MIS5e sequence. (a) *North Greenland Ice Core Project members* [2004] (blue) and *NEEM community members* [2013] δ^{18}O sections (purple). (b) ODP976 *G. bulloides* δ18O$_{ivc}$. (c) ODP976 *G. bulloides* Mg/Ca temperature profile. (d) ODP976 δ18O$_{sw}$ profile calculated from δ^{18}O$_{ivc}$ and Mg/Ca temperatures shown in Figures 6b and 6c. (e) *G. bulloides* Mg/Ca temperature profile and (f) δ18O$_{sw}$ profile of core MD01-2444 from the western Iberian margin on their published timescales [*Skinner and Shackleton*, 2006]. (g) Speleothem δ^{18}O profile from Dongge Cave [*Kelly et al.*, 2006] with ^{230}Th datums marked along bottom *x* axis. Red line is unlagged orbital precession highlighting deviation of monsoon strength from insolation forcing during the prolonged weak monsoon interval (WMI) of T2.

agrees with the temporal extent of the weak monsoon interval (WMI) recorded in the Dongge speleothem $\delta^{18}O$ profile at the end of MIS6 that was suggested to be connected with the H11 cold phase in the North Atlantic and was dated to between 135.5 ± 1.0 kyr to 129.0 ± 1.0 kyr (Figure 6g) [*Cheng et al.*, 2006; *Kelly et al.*, 2006]. However, the negative $\delta^{18}O_{sw}$ anomaly at ODP976 started at 132.6 kyr which suggests the H11 low-salinity waters reached ODP976 about 3 kyr after the onset of subpolar conditions in the North Atlantic. Fine-scale paleorecords in the western Mediterranean indeed suggested that the advection of the low-salinity waters was discontinuous during Heinrich events [*Frigola et al.*, 2008] and the delayed incursion of H11 cold/low-salinity water at ODP976 may be a reflection of the discontinuous water advection.

A further compelling feature of T2 at ODP976 is the abrupt warming by 6°C centered at 128.8 kyr that marked the end of H11and onset of MIS5e (Figure 6). Similar high-amplitude warming was documented at other Northeast Atlantic sites [*Oppo et al.*, 2006; *Sánchez-Goñi et al.*, 2012] and was accompanied by a rapid onset of last interglacial conditions in western Europe and an accelerated expansion of temperate forests [*Sánchez-Goñi et al.*, 2012, 2013]. The abrupt decrease of $\delta^{18}O$ in the Dongge speleothem record reflects the coincident shift of monsoon activity in Asia to full interglacial strength at this time (Figure 6g) and the reestablishment of the dominant solar radiation control of Asian monsoon strength that was suppressed during H11 [*Wang et al.*, 2001; *Kelly et al.*, 2006]. The radiometrically dated speleothem timescale suggests the monsoons reached full strength within 800 years, with the first half of the recovery occurring within less than 60 years [*Kelly et al.,* 2006; *Cheng et al.*, 2009]. The T2 warming at western Iberian core MD01-2444 [*Skinner and Shackleton*, 2006] was lower in amplitude and more gradual reaching peak MIS5e temperatures approximately 2.5–3 kyr after peak temperatures were recorded at ODP976. High-resolution marine and terrestrial paleoprofiles from the Northeast Atlantic farther north indicate strong and rapid warming in western Europe at around 131 kyr, several millennia before warmest temperatures were recorded at midlatitude sites in the Northeast Atlantic [*Sánchez-Goñi et al.*, 2012]. Hence, the abrupt warming at ODP976 at the onset of MIS5e fits with the terrestrial warming and rapid development of temperate forests indicated in pollen records. Extending the speleothem timescale of the coincident abrupt strengthening of Asian monsoons to the ODP976 profiles would suggest that MIS5e warmth in the region was initiated within less than one millennium.

The MIS5e section at ODP976 displays warm-cold oscillations that commenced with rebounding Mg/Ca temperatures after the early MIS5e peak warmth by 3°C. Oscillations are also seen in the MD01-2444 temperature profile at the Iberian margin [*Skinner and Shackleton*, 2006] and in the Antro del Corchia and La Chaise speleothem $\delta^{18}O$ profiles from Italy and southern France [*Drysdale et al.*, 2009; *Couchoud et al.*, 2009]. Planktic Mg/Ca and geochemical proxies for terrestrial sedimentation at the southern tip of Greenland likewise indicate rebounding marine temperatures and an oscillatory behavior of the Greenland ice sheet and meltwater runoff during MIS5e [*Hillaire-Marcel et al.*, 2001; *Carlson et al.*, 2008; *Irvali et al.*, 2012]. Surface water cooling and freshening in the Northwest Atlantic at 126 kyr [*Irvali et al.*, 2012] coincided with lowered benthic foraminiferal $\delta^{13}C$ and sedimentologic evidence of reduced near-bottom flow speeds both diagnosing weakened deep water circulation [*Hodell et al.*, 2009; *Galaasen et al.*, 2014]. The incursion of cooling and freshening at ODP976 (Figures 6c and 6d) around the same time suggests a possibility that the MIS5e oscillations may have been part of a pervasive climatic variability affecting the northern North Atlantic at the basin scale, plausibly involving freshwater surges from continuing disintegration of Northern Hemisphere ice sheets during early MIS5e and the Arctic [*Hillaire-Marcel et al.*, 2001; *Carlson et al.*, 2008; *Nicholl et al.*, 2012; *Galaasen et al.*, 2014]. Sedimentological, micropaleontological, and stable isotope evidence from the Nordic Seas indeed revealed that conditions favorable of significant convective activity and deep water formation were delayed until the later stages of MIS5e [*Van Nieuwenhove et al.*, 2011; *Bauch*, 2013; *Van Nieuwenhove et al.*, 2013].

The Saalian (MIS6) ice sheet in Eurasia extended farther east into Siberia than that of the late Weichselian (MIS2) [*Ehlers et al.*, 2013], and its melting apparently continued well beyond the oxygen isotope termination T2 while substantially affecting the MIS5e climatology in the northern North Atlantic region [*Van Nieuwenhove and Bauch*, 2008; *Van Nieuwenhove et al.*, 2011; *Bauch*, 2013]. The North American Illinoian Stage (MIS6) ice sheet likewise exceeded the Wisconsin (MIS2) ice sheet in size but the difference between both was rather small [*Curry et al.*, 2011]. Numerical models [*Montoya et al.,* 2000; *Kaspar et al.,* 2005] suggest the largest warming during MIS5e occurred over Eurasia and Greenland which would have

sustained the meltwater flow from Greendland, Eurasia, and the Arctic [*Otto-Bliesner et al.*, 2006; *van de Berg et al.*, 2011] several millennia into MIS5e. This ultimately delayed full-strength convection and the advection of warm North Atlantic waters to the Nordic Seas until the later stages of MIS5e [*Van Nieuwenhove et al.*, 2011; *Govin et al.*, 2012; *Bauch*, 2013].

The existence or absence of a Younger Dryas-type climatic rebound during T2 is discussed controversially [*Carlson*, 2008; *Bauch et al.*, 2012; *Sánchez-Goñi et al.*, 2012], but from the structure of the ODP976 Mg/Ca temperature profile one would be able to argue that the abrupt temperature increase after H11 at ODP976 and the following cooling in early MIS5e mimic the B/A warming after H1 and subsequent Younger Dryas cooling during T1. Evidence for early MIS5e freshening and cooling across the North Atlantic [*Irvali et al.*, 2012; *Nicholl et al.*, 2012] and coeval weakening of convective activity and deep water circulation [*Hodell et al.*, 2009; *Galaasen et al.*, 2014] indeed suggest that this was a YD-type climatic rebound that was shifted into the early stages of the last interglacial.

5. Conclusions

The structure of the δ^{18}O data profiles from planktic foraminifera at ODP976 was nearly identical during the last two glacial-interglacial transitions (T1 and T2). While this would seem to indicate that climatic developments at the end of the last two glacial periods were closely correlated, the ODP976 planktic Mg/Ca profiles display different temperature progressions. T1 displays a series of transient temperature oscillations, such as the polar conditions during the H1 meltwater event and the Younger Dryas that were intersected by the warm B/A period, reflecting variable freshwater perturbation and alternating weak and strong states of the AMOC. Such temperature oscillations were absent at ODP976 at the end of the penultimate glacial period and instead T2 was marked by an extended period of polar conditions coincident with H11. The abrupt single-step warming at the end of H11 by 6°C mimicked the sudden B/A warming during T1 and at the same time marked the onset of full interglacial MIS5e conditions. This development is reflected in European terrestrial pollen sequences and speleothem records from Asia that display T2 as a rapid warming across western Europe to interglacial levels with accelerated spreading of temperate forests [*Sánchez-Goñi et al.*, 2005, 2012] and an abrupt single-step increase of Asian monsoon activity to full interglacial levels [*Kelly et al.*, 2006; *Cheng et al.*, 2009]. Using the radiometrically dated speleothem sequences of the abrupt Asian Monsoon Termination II [*Kelly et al.*, 2006] as a reference for the single-step post-H11 Mg/Ca temperature shift at ODP976 suggests that subpolar conditions in the Northeast Atlantic region were terminated abruptly at 129 kyr and full interglacial temperatures were reached within less than a millennium. The late establishment of interglacial warmth at high northern latitudes and full-strength deep water convection several millennia after the onset of MIS5e plausibly resulted from the continuing disintegration of the large Saalian Stage (MIS6) ice sheet in Eurasia that extended far into Siberia [*Ehlers et al.*, 2013] where conditions previously were thought unfavorable for ice accumulation [*Anisimov et al.*, 2006; *Basilyan et al.*, 2008]. Disintegration of its large ice volume at the end of the penultimate glacial perturbed the high-latitude climate and sustained subpolar conditions in the Nordic Seas until several millennia after the onset of interglacial conditions at lower latitudes [*Van Nieuwenhove et al.*, 2011; *Bauch*, 2013; *Van Nieuwenhove et al.*, 2013].

The structure of the ODP976 Mg/Ca temperature profile at the end of MIS6 would be consistent with the suggestion that the abrupt post-H11 temperature increase and the following cooling in the early MIS5e were the equivalents of the B/A warming and Younger Dryas cooling during T1. Freshening and cooling across the North Atlantic [*Irvali et al.*, 2012; *Nicholl et al.*, 2012] and coeval weakening of convective activity and deep water circulation [*Hodell et al.*, 2009; *Galaasen et al.*, 2014] indeed mimicked YD conditions but would have been shifted into the interglacial regime of early MIS5e.

Acknowledgments

This study received financial support from the European Union's Seventh Framework program collaborative project "Climate change—Learning from the past climate (Past4Future)" under grant agreement 243908. The coordinator Dorthe Dahl-Jensen and Henning Thing are thanked for their continuing leadership and efforts of running the project. We are indebted to Isabel Cacho, Pere Masqué, Bruno Malaize, and Laurent Londeix who shared data with us. Nathalie Combourieu-Nebout and Belen Martrat are thanked for sharing samples and many discussions. Tom Cronin, Jürgen Ehlers, and Brandon Curry shared their insight into late Pleistocene North American and Eurasian ice sheet developments. Our colleagues of the Past4Future project are thanked for the multiple discussions during the Past4Future project meetings. The data for this paper are available at the PANGAEA Data Publisher for Earth & Environmental Science (http://www.pangaea.de/).

References

Allen, J. R., and B. Huntley (2009), Last Interglacial palaeovegetation, palaeoenvironments and chronology: A new record from Lago Grande di Monticchio, southern Italy, *Quat. Sci. Rev.*, *28*(15), 1521–1538.

Anisimov, M. A., V. Y. Tumskoy, and V. V. Ivanova (2006), Massive ice of the New Siberian Islands as a relict of ancient glaciation, *Materialy Glatsiologicheskih Issledovaniy*, *101*, 143–145.

Antonov, J. I., D. Seidov, T. P. Boyer, R. A. Locarnini, A. V. Mishonov, H. E. Garcia, and D. R. Johnson (2010), World Ocean Atlas 2009, Salinity, in *NOAA Atlas NESDIS 69*, vol. 2, edited by S. Levitus, pp. 184, U.S. Gov. Print. Off., Washington, D. C.

Arbuszewski, J., P. deMenocal, A. Kaplan, and E. C. Farmer (2010), On the fidelity of shell-derived $\delta^{18}O_{seawater}$ estimates, *Earth Planet. Sci.*, *200*, 185–196.

Arz, H. W., F. Lamy, A. Ganopolski, N. Nowaczyk, and J. Pätzold (2007), Dominant Northern Hemisphere climate control over millennial-scale glacial sea-level variability, *Quat. Sci. Rev.*, *26*(3), 312–321.
Bakker, P., et al. (2013), Last interglacial temperature evolution—A model inter-comparison, *Clim. Past*, *9*, 605–619.
Bárcena, M. A., et al. (2004), Planktonic response to main oceanographic changes in the Alboran Sea (western Mediterranean) as documented in sediment traps and Surface sediments, *Mar. Micropaleontol.*, *53*, 423–445.
Bard, E., F. Rostek, J. L. Turon, and S. Gendreau (2000), Hydrological impact of Heinrich events in the subtropical northeast Atlantic, *Science*, *289*(5483), 1321–1324.
Bard, E., G. Delaygue, F. Rostek, F. Antonioli, S. Silenzi, and D. P. Schrag (2002), Hydrological conditions over the western Mediterranean basin during the deposition of the cold Sapropel 6 (ca. 175 kyr BP), *Earth Planet. Sci. Lett.*, *202*(2), 481–494.
Bard, E., F. Rostek, and G. Ménot-Combes (2004), Radiocarbon calibration beyond 20,000 ^{14}C yr B.P. by means of planktonic foraminifera of the Iberian Margin, *Quat. Res.*, *61*(2), 204–14.
Bard, E., B. Hamelin, and D. Delanghe-Sabatier (2010), Deglacial meltwater pulse 1B and Younger Dryas sea levels revisited with boreholes at Tahiti, *Science*, *327*(5970), 1235–1237.
Barker, S., M. Greaves, and H. Elderfield (2003), A study of cleaning procedures used for foraminiferal Mg/Ca paleothermometry, *Geochem., Geophys., Geosyst.*, *4*(9), 8407, doi:10.1029/2003GC000559.
Bar-Matthews, M., and A. Ayalon (2004), Speleothems as palaeoclimate indicators, a case study from Soreq Cave located in the Eastern Mediterranean Region, Israel, in *Past Climate Variability Through Europe and Africa*, pp. 363–391, Springer, Netherlands.
Bar-Matthews, M., A. Ayalon, M. Gilmour, A. Matthews, and C. J. Hawkesworth (2003), Sea–land oxygen isotopic relationships from planktonic foraminifera and speleothems in the Eastern Mediterranean region and their implication for paleorainfall during interglacial intervals, *Geochim. Cosmochim. Acta*, *67*(17), 3181–3199.
Basilyan, A. E., M. A. Anisimov, and P. A. Nikolsky (2008), Pleistocene glaciation of the New Siberia Islands—No doubts left, Information Bull. Int. Phys. Year 2007/2008 News, 12:7–9.
Bauch, H. A. (2013), Interglacial climates and the Atlantic meridional overturning circulation: is there an Arctic controversy?, *Quat. Sci. Rev.*, *63*, 1–22.
Bauch, H. A., E. S. Kandiano, and J. P. Helmke (2012), Contrasting ocean changes between the subpolar and polar North Atlantic during the past 135 ka, *Geophys. Res. Lett.*, *39*, L11604, doi:10.1029/2012GL051800.
Bemis, B. E., H. J. Spero, and R. C. Thunell (2002), Using species-specific paleotemperature equations with foraminifera: A case study in the Southern California Bight, *Mar. Micropaleontol.*, *46*(3), 405–430.
Berger, A., and M. F. Loutre (2002), An exceptionally long interglacial ahead?, *Science*, *297*, 1287–1288.
Blunier, T., et al. (1998), Asynchrony of Antarctic and Greenland climate change during the last glacial period, *Nature*, *394*(6695), 739–743.
Bond, G., B. Kromer, J. Beer, R. Muscheler, M. N. Evans, W. Showers, S. Hoffmann, R. Lotti-Bond, I. Hajdas, and G. Bonani (2001), Persistent solar influence on North Atlantic climate during the Holocene, *Science*, *294*, 2130–2136.
Boyle, E. A. (1983), Manganese carbonate overgrowths on foraminifera tests, *Geochim. Cosmochim. Acta*, *47*(19), 1815–1819.
Boyle, E. A., and L. D. Keigwin (1985), Comparison of Atlantic and Pacific paleochemical records for the last 215,000 years: Changes in deep ocean circulation and chemical inventories, *Earth Planet. Sci. Lett.*, *76*(1), 135–150.
Brauer, A., C. Günter, S. J. Johnsen, and J. F. W. Negendank (2000), Land-ice teleconnections of cold climatic periods during the last Glacial/Interglacial transition, *Clim. Dyn.*, *16*(2–3), 229–239.
Cacho, I. (1999), Dansgaard-Oeschger and Heinrich event imprints in the Alboran Sea paleotemperatures, *Paleoceanography*, *14*, 698–705, doi:10.1029/1999PA900044.
Cacho, I., J. O. Grimalt, C. Pelejero, M. Canals, F. J. Sierro, J. A. Flores, and N. Shackleton (1999), Dansgaard-Oeschger and Heinrich event imprints in Alboran Sea paleotemperatures, *Paleoceanography*, *14*(6), 698–705.
Cacho, I., J. O. Grimalt, F. J. Sierro, N. Shackleton, and M. Canals (2000), Evidence for enhanced Mediterranean thermohaline circulation during rapid climatic coolings, *Earth Planet. Sci. Lett.*, *183*(3), 417–429.
Cacho, I., et al. (2001), Variability of the western Mediterranean Sea surface temperature during the last 25,000 years and its connection with the Northern Hemisphere climatic changes, *Paleoceanography*, *16*, 40–52, doi:10.1029/2000PA000502.
Cacho, I., J. O. Grimalt, and M. Canals (2002), Response of the western Mediterranean Sea to rapid climatic variability during the last 50,000 years: A molecular biomarker approach, *J. Mar. Syst.*, *33-34*, 253–272.
Cacho, I., N. Shackleton, H. Elderfield, F. J. Sierro, and J. O. Grimalt (2006), Glacial rapid variability in deep-water temperature and δ^{18}O from the Western Mediterranean Sea, *Quat. Sci. Rev.*, *25*(23), 3294–3311.
Carlson, A. E. (2008), Why there was not a Younger Dryas-like event during the Penultimate Deglaciation, *Quat. Sci. Rev.*, *27*, 882–887.
Carlson, A. E., and P. U. Clark (2012), Ice sheet sources of sea level rise and freshwater discharge during the last deglaciation, *Rev. Geophys.*, *50*, RG4007, doi:10.1029/2011RG000371.
Carlson, A. E., J. S. Stoner, J. P. Donnelly, and C. Hillaire-Marcel (2008), Response of the southern Greenland Ice Sheet during the last two degalciations, *Geology*, *36*, 359–362.
Cayre, O., Y. Lancelot, E. Vincent, and M. A. Hall (1999), Paleoceanographic reconstructions from planktonic foraminifera off the Iberian Margin: Temperature, salinity, and Heinrich events, *Paleoceanography*, *14*(3), 384–396, doi:10.1029/1998PA900027.
Cheng, H., et al. (2006), A penultimate glacial monsoon record from Hulu Cave and two-phase glacial terminations, *Geology*, *34*(3), 217–220.
Cheng, H., et al. (2009), Ice age terminations, *Science*, *326*, 248–252.
Clark, P. U., et al. (2012), Global climate evolution during the last deglaciation, *Proc. Nat. Acad. Sci.*, *109*(19), E1134–E1142.
Comas, M. C., et al. (1996), *Proceedings of the Ocean Drilling Program*, *Initial Rep.*, vol. 161, Ocean Drilling Program, College Station, Tex.
Combourieu-Nebout, N., et al. (1999), Quaternary marine and continental paleoenvironments in the western Mediterranean (Site 976, Alboran Sea): Palynological evidence, in *Proceedings of the Ocean Drilling Program*, *Sci. Results*, vol. 161, edited by R. Zahn, M. C. Comas, and A. Klaus, pp. 457–468, Ocean Drilling Program, College Station, Tex.
Combourieu-Nebout, N., et al. (2002), Enhanced aridity and atmospheric high-pressure stability over the western Mediterranean during the North Atlantic cold events of the past 50 ky, *Geology*, *30*(10), 863–866.
Combourieu-Nebout, N., et al. (2009), Rapid climatic variability in the west Mediterranean during the last 25,000 years from high resolution pollen data, *Clim. Past*, *5*(3), 503.
Condron, A., and P. Winsor (2012), Meltwater routing and the Younger Dryas, *Proc. Natl. Acad. Sci. U.S.A.*, *109*, 19,928–19,933.
Couchoud, I., D. Genty, D. Hoffmann, R. N. Drysdale, and D. Blamart (2009), Millennial-scale climate variability during the Last Interglacial recorded in a speleothem from south-western France, *Quat. Sci. Rev.*, *28*(27), 3263–3274.
Curry, B. B., D. A. Grimley, and E. D. McKay III (2011), Quaternary Glaciations in Illinois, in *Developments in Quaternary Science*, vol. 15, edited by J. Ehlers, P. L. Gibbard, and P. D. Hughes, pp. 467–487, Elsevier, Amsterdam, Netherlands.

de Kaenel, E., W. G. Siesse, and A. Murat (1999), Pleistocene calcareous nannofossil biostratigraphy and the western Mediterranean sapropels, Sites 974 to 977 and 979, in *Proceedings of the Ocean Drilling Program, Sci. Results*, vol. 161, edited by R. Zahn, M. C. Comas, and A. Klaus, pp. 159–183, Ocean Drilling Program, College Station, Tex.

de Villiers, S., M. Greaves, and H. Elderfield (2002), An intensity ratio calibration method for the accurate determination of Mg/Ca and Sr/Ca of marine carbonates by ICP-AES, *Geochem., Geophys., Geosyst.*, *3*(1), 1001, doi:10.1029/2001GC000169.

deMenocal, P., and L. Baker (2000), Benthic stable isotope data from sites 1014 and 1020 (0.6-1.2 MA), in *Proceedings of the Ocean Drilling Program, Sci. Results*, vol. 167, pp. 145–150, Ocean Drilling Program, College Station, Tex.

Deschamps, P., et al. (2012), Ice-sheet collapse and sea-level rise at the Bolling warming 14,600-years ago, *Nature*, *483*, 559–564.

Di Stefano, A., et al. (2015), Mediterranean coccolith ecobiostratigraphy since the penultimate Glacial (the last 145,000 years) and ecobioevent traceability, *Mar. Micropaleontol.*, *115*, 24–38.

Di Stefano, E., A. Incarbona, R. Sprovieri, and S. Ferraro (2014), Ten years of paleoceanographic studies at ODP Site 963 (Central Mediterranean Sea), *Open Paleontol. J.*, *5*, 10–19.

Dixit, Y., D. A. Hodell, R. Sinha, and C. A. Petrie (2014), Abrupt weakening of the Indian summer monsoon at 8.2 kyr BP, *Earth Planet. Sci. Lett.*, *391*, 16–23.

Dos Santos, R. A., M. I. Spooner, T. Barrows, P. de Deckker, J. S. Sinninghe Damsté, and S. Schouten (2013), Comparison of organic (Uk'37, TEXH86, LDI) and faunal proxies (foraminiferal assemblages) for reconstruction of late Quaternary sea surface temperature variability from offshore southeastern Australia, *Paleoceanography*, *28*, 377–387, doi:10.1002/palo.20035.

Drysdale, R. N., G. Zanchetta, G. Hellstrom, A. E. Fallick, and J. Zhao (2005), Stalagmite evidence for the onset of the Last Interglacial in southern Europe at 129 ± 1 ka, *Geophys. Res. Lett.*, *32*, L24708, doi:10.1029/2005GL024658.

Drysdale, R. N., et al. (2007), Stalagmite evidence for the precise timing of North Atlantic cold events during the early last glacial, *Geology*, *35*(1), 77–80.

Drysdale, R. N., et al. (2009), Evidence for obliquity forcing of Glacial Termination II, *Science*, *325*(5947), 1527.

Dykoski, C. A., et al. (2005), A high-resolution, absolute-dated Holocene and deglacial Asian Monsoon record from Dongge Cave, China, *Earth Planet. Sci. Lett.*, *233*(1), 71–86.

Ehlers, J., V. Astakhov, P. L. Gibbard, J. Mangerud, and J. I. Svendsen (2013), Middle Pleistocene Glaciations in Eurasia, in *Encyclopedia of Quaternary Science*, edited by S. A. Elias, pp. 172–179, Elsevier, Amsterdam.

Elderfield, H., and G. Ganssen (2000), Past temperature and $\delta^{18}O$ of surface ocean waters inferred from foraminiferal Mg/Ca ratios, *Nature*, *405*, 442–445.

Ellison, C. R., M. R. Chapman, and I. R. Hall (2006), Surface and deep ocean interactions during the cold climate event 8200 years ago, *Science*, *312*(5782), 1929–1932.

Eynaud, F., L. de Abreu, A. Voelker, J. Schönfeld, E. Salgueiro, J. L. Turon, A. Penaud, S. Toucanne, and F. Naughton (2009), Position of the polar front along the western Iberian margin during key cold episodes of the last 45 ky, *Geochem., Geophys., Geosyst.*, *10*(7), 1525–2027.

Ferguson, J. E., G. M. Henderson, M. Kucera, and R. E. M. Rickaby (2008), Systematic change of foraminiferal Mg/Ca ratios across a strong salinity gradient, *Earth Planet. Sci. Lett.*, *265*, 153–166.

Frigola, J., A. Moreno, I. Cacho, M. Canals, F. J. Sierro, J. A. Flores, and J. O. Grimalt (2008), Evidence of abrupt changes in western Mediterranean Deep Water circulation during the last 50 kyr: A high-resolution marine record from the Balearic Sea, *Quat. Int.*, *181*(1), 88–104.

Galaasen, E. V., et al. (2014), Rapid reductions in North Atlantic deep water during the peak of the last interglacial period, *Science*, *343*(6175), 1129–1132.

Ganssen, G. M., and D. Kroon (2000), The isotopic signature of planktonic foraminifera from NE Atlantic surface sediments implications for the reconstruction of past oceanic conditions, *J. Geol. Soc.*, *157*, 693–699.

Gasse, F., and E. Van Campo (1994), Abrupt post-glacial climate events in West Asia and North Africa monsoon domains, *Earth Planet. Sci. Lett.*, *126*(4), 435–456.

Genty, D., D. Blamart, R. Ouahdi, M. Gilmour, A. Baker, J. Jouzel, and S. Van-Exter (2003), Precise dating of Dansgaard–Oeschger climate oscillations in western Europe from stalagmite data, *Nature*, *421*(6925), 833–837.

Genty, D., D. Blamart, B. Ghaleb, V. Plagnes, C. Causse, M. Bakalowicz, and F. Bourges (2006), Timing and dynamics of the last deglaciation from European and North African δ13C stalagmite profiles—Comparison with Chinese and South Hemisphere stalagmites, *Quat. Sci. Rev.*, *25*(17), 2118–2142.

Gherardi, J. M., L. Labeyrie, S. Nave, R. François, J. F. McManus, and E. Cortijo (2009), Glacial-interglacial circulation changes inferred from 231Pa/230Th sedimentary record in the North Atlantic region, *Paleoceanography*, *24*, PA2204, doi:10.1029/2008PA001696.

Goslar, T., T. Kuc, M. Ralska-Jasiewiczowa, K. Rózánski, M. Arnold, E. Bard, and A. Walanus (1993), High-resolution lacustrine record of the Late Glacial/Holocene transition in Central Europe, *Quat. Sci. Rev.*, *12*(5), 287–294.

Gouzy, A., B. Malaizé, C. Pujol, and K. Charlier (2004), Climatic "pause" during Termination II identified in shallow and intermediate waters off the Iberian margin, *Quat. Sci. Rev.*, *23*, 1523–1528.

Govin, A., et al. (2012), Persistent influence of ice sheet melting on high northern latitude climate during the early Last Interglacial, *Clim. Past*, *8*(2), 483–507.

Grant, K. M., E. J. Rohling, M. Bar-Matthews, A. Ayalon, M. Medina-Elizalde, C. B. Ramsey, and A. P. Roberts (2012), Rapid coupling between ice volume and polar temperature over the past 150,000 years, *Nature*, *491*(7426), 744–747.

Greaves, M., N. Caillon, H. Rebaubier, G. Bartoli, S. Bohaty, I. Cacho, and P. A. Wilson (2008), Interlaboratory comparison study of calibration standards for foraminiferal Mg/Ca thermometry, *Geochem., Geophys., Geosyst.*, *9*, Q08010, doi:10.1029/2008GC001974.

Gyldenfeldt, A. B. V., J. Carstens, and J. Meincke (2000), Estimation of the catchment area of a sediment trap by means of current meters and foraminiferal tests, *Deep Sea Res., Part II*, *47*(9), 1701–1717.

Heinrich, H. (1988), Origin and consequences of cyclic ice rafting in the Northeast Atlantic Ocean during the past 130,000 years, *Quat. Res.*, *29*, 142–152.

Hemming, S. R. (2004), Heinrich events: Massive late Pleistocene detritus layers of the North Atlantic and their global climate imprint, *Rev. Geophys.*, *42*, RG1005, doi:10.1029/2003RG000128.

Hernández-Almeida, I., et al. (2011), Microplankton response to environmental conditions in the Alboran Sea (western Mediterranean): One year sediment trap record, *Mar. Micropaleontol.*, *78*, 14–24.

Hillaire-Marcel, C., A. de Vernal, G. Bilodeau, and A. J. Weaver (2001), Absence of deep-water formation in the Labrador Sea during the last interglacial period, *Nature*, *410*, 1073–1077, doi:10.1038/35074059.

Hodell, D. A., et al. (2009), Surface and deepwater hydrography on Gardar Drift (Iceland Basin) during the last interglacial period, *Earth Planet. Sci. Lett.*, *288*, 10–19.

Hodell, D., S. Crowhurst, L. Skinner, P. C. Tzedakis, V. Margari, J. E. T. Channell, G. Kamenov, S. Maclachlan, and G. Rothwell (2013), Response of the Iberian Margin sediments to orbital and suborbital forcing over the past 420 ka, *Paleoceanography*, *28*, 185–199, doi:10.1002/palo.20017.

Hoogakker, B. A., G. P. Klinkhammer, H. Elderfield, E. J. Rohling, and C. Hayward (2009), Mg/Ca paleothermometry in high salinity environments, *Earth Planet. Sci. Lett.*, *284*(3), 583–589.

Hughen, K., J. Southon, S. Lehman, C. Bertrand, and J. Turnbull (2006), Marine-derived 14C calibration and activity record for the past 50,000 years updated from the Cariaco Basin, *Quat. Sci. Rev.*, *25*(23–24), 3216–27.

Huguet, C., B. Martrat, J. O. Grimalt, J. S. Sinninghe Damsté, and S. Schouten (2011), Coherent millennial scale patterns in Uk'37 and TEX H86 temperature records during the penultimate interglacial-to-glacial cycle in the western Mediterranean, *Paleoceanography*, *26*, PA2218, doi:10.1029/2010PA002048.

Incarbona, A., E. Di Stefano, R. Sprovieri, S. Bonomo, N. Pelosi, and M. Sprovieri (2010), Millennial-scale paleoenvironmental changes in the central Mediterranean during the last interglacial: Comparison with European and North Atlantic records, *Geobios*, *43*(1), 111–122.

Incarbona, A., P. Ziveri, N. Sabatino, D. S. Manta, and M. Sprovieri (2011), Conflicting coccolithophore and geochemical evidence for productivity levels in the Eastern Mediterranean sapropel S1, *Mar. Micropaleontol.*, *81*(3), 131–143.

Irvali, N., et al. (2012), Rapid switches in subpolar North Atlantic hydrography and climate during the Last Interglacial (MIS5e), *Paleoceanography*, *27*, PA2207, doi:10.1029/2011PA002244.

Jackson, C. S., O. Marchal, Y. Liu, S. Lu, and W. G. Thompson (2010), A box model test of the freshwater forcing hypothesis of abrupt climate change and the physics governing ocean stability, *Paleoceanography*, *25*, PA4222, doi:10.1029/2010PA001936.

Jonkers, L., S. van Heuven, R. Zahn, and F. J. C. Peeters (2013), Seasonal patterns of shell flux, δ^{18}O and δ^{13}C of small and large N. pachyderma (s) and G. bulloides in the subpolar North Atlantic, *Paleoceanography*, *48*, 164–174, doi:10.1002/palo.20018.

Kaspar, F., et al. (2005), A model-data comparison of European temperatures in the Eemian interglacial, *Geophys. Res. Lett.*, *32*, L11703, doi:10.1029/2005GL022456.

Kelly, M. J., et al. (2006), High resolution characterization of the Asian Monsoon between 146,000 and 99,000 years B.P. from Dongge Cave, China and global correlation of events surrounding Termination II, *Paleaeogeogr., Palaeoclimatol., Palaeoecol.*, *236*, 20–38.

Kuhlemann, J., E. J. Rohling, I. Krumrei, P. Kubik, S. Ivy-Ochs, and M. Kucera (2008), Regional synthesis of Mediterranean atmospheric circulation during the Last Glacial Maximum, *Science*, *321*(5894), 1338–1340.

Laepple, T., and P. Huybers (2013), Reconciling discrepancies between Uk37 and Mg/Ca reconstructions of Holocene marine temperature variability, *Earth Planet. Sci. Lett.*, *375*, 418–429.

Laepple, T., and P. Huybers (2014), Global and regional variability in marine surface temperatures, *Geophys. Res. Lett.*, *41*, 2528–2534, doi:10.1002/2014GL059345.

Lea, D. W., T. A. Mashiotta, and H. J. Spero (1999), Controls on magnesium and strontium uptake in planktonic foraminifera determined by live culturing, *Geochim. Cosmochim. Acta*, *63*, 2369–2379.

Leduc, G., R. Schneider, J. H. Kim, and G. Lohmann (2010), Holocene and Eemian sea surface temperature trends as revealed by alkenone and Mg/Ca paleothermometry, *Quat. Sci. Rev.*, *29*, 989–1004.

Li, Y., N. A. Wang, X. Zhou, C. Zhang, and Y. Wang (2014), Synchronous or asynchronous Holocene Indian and East Asian summer monsoon evolution: A synthesis on Holocene Asian summer monsoon simulations, records and modern monsoon indices, *Global Planet. Change*, *116*, 30–40.

Lisiecki, L. E., and M. E. Raymo (2004), A Pliocene-Pleistocene stack of 57 globally distributed benthic δ^{18}O records, *Paleoceanography*, *20*, PA1018, doi:10.1029/2003PA000999.

Liu, W., Z. Liu, and A. Hu (2013), The stability of an evolving Atlantic meridional overturning circulation, *Geophys. Res. Lett.*, *40*, 1562–1568, doi:10.1002/grl.50365.

Liu, Z., B. L. Otto-Bliesner, F. He, E. C. Brady, R. Tomas, P. U. Clark, and J. Cheng (2009), Transient simulation of last deglaciation with a new mechanism for Bølling-Allerød warming, *Science*, *325*(5938), 310–314.

Locarnini, R. A., et al. (2010), *World Ocean Atlas 2009, Volume 1: Temperature*, *NOAA Atlas NESDIS*, vol. 68, edited by S. Levitus, 184 pp., U.S. Gov. Print. Off., Washington, D. C.

Loulergue, L., A. Schilt, R. Spahni, V. Masson-Delmotte, T. Blunier, B. Lemieux, J.-M. Barnola, D. Raynaud, T. F. Stocker, and J. Chapellaz (2008), Orbital and millennial-scale features of atmospheric CH_4 over the past 800,000 years, *Nature*, *453*(7193), 383–386.

Marchal, O., I. Cacho, T. F. Stocker, J. O. Grimalt, E. Calvo, B. Martrat, and E. Jansen (2002), Apparent long-term cooling of the sea surface in the northeast Atlantic and Mediterranean during the Holocene, *Quat. Sci. Rev.*, *21*(4), 455–483.

Marret, F., and K. A. Zonneveld (2003), Atlas of modern organic-walled dinoflagellate cyst distribution, *Rev. Palaeobot. Palynol.*, *125*(1), 1–200.

Martrat, B., et al. (2004), Abrupt temperature changes in the western Mediterranean over the past 250,000 years, *Science*, *306*(5702), 1762.

Martrat, B., J. O. Grimalt, N. J. Shackleton, L. de Abreu, M. A. Hutterli, and T. F. Stocker (2007), Four climate cycles of recurring deep and surface water destabilizations on the Iberian Margin, *Science*, *317*(502), doi:10.1126/science.1139994.

Martrat, B., P. Jiménez-Amat, R. Zahn, and J. O. Grimalt (2014), Similarities and dissimilarities between the last two deglaciations and interglaciations in the North Atlantic region, *Quat. Sci. Rev.*, *99*, 122–134.

Masqué, P., et al. (2003), Accumulation rates of major constituents of hemipelagic sediments in the deep Alboran Sea: A centennial perspective of sedimentary dynamics, *Mar. Geol.*, *193*(3), 207–233.

Masson-Delmotte, V., B. Stenni, and J. Jouzel (2004), Common millennial-scale variability of Antarctic and Southern Ocean temperatures during the past 5000 years reconstructed from the EPICA Dome C ice core, *Holocene*, *14*(2), 145–151.

Masson-Delmotte, V., et al. (2006), Past and future polar amplification of climate change: Climate model intercomparisons and ice-core constraints, *Clim. Dyn.*, *26*, 513–529.

McDermott, F. (2004), Palaeo-climate reconstruction from stable isotope variations in speleothems: A review, *Quat. Sci. Rev.*, *23*(7), 901–918.

McManus, J. F., G. C. Bond, W. S. Broecker, S. Johnsen, L. Labeyrie, and S. Higgins (1994), High-resolution climate records from the North Atlantic during the last interglacial, *Nature*, *371*, 326–329.

Mohtadi, M., M. Prange, D. W. Oppo, R. De Pol-Holz, U. Merkel, X. Zhang, S. Steinke, and A. Lückge (2014), North Atlantic forcing of tropical Indian Ocean climate, *Nature*, *509*(7498), 76–80.

Montoya, M., et al. (2000), Climate simulation for 125 kyr BP with a Coupled Ocean–Atmosphere General Circulation Model, *J. Clim.*, *13*(6), 1057–1072.

Moreno, A., I. Cacho, M. Canals, J. O. Grimalt, M. F. Sánchez-Goñi, N. Shackleton, and F. J. Sierro (2005), Links between marine and atmospheric processes oscillating on a millennial time-scale. A multi-proxy study of the last 50,000 yr from the Alboran Sea (Western Mediterranean Sea), *Quat. Sci. Rev.*, *24*(14–15), 1623.

Moreno, A., H. Stoll, M. Jiménez-Sánchez, I. Cacho, B. Valero-Garcés, E. Ito, and R. L. Edwards (2010), A speleothem record of glacial (25–11.6 kyr BP) rapid climatic changes from northern Iberian Peninsula, *Global Planet. Change*, *71*(3), 218–231.

Mortyn, P. G., and C. D. Charles (2003), Planktonic foraminiferal depth habitat and δ^{18}O calibrations: Plankton tow results from the Atlantic sector of the Southern Ocean, *Paleoceanography*, *18*(2), 1037, doi:10.1029/2001PA000637.
Naughton, F., et al. (2009), Wet to dry trend in north-western Iberia within Heinroch events, *Earth Planet. Sci. Lett.*, *284*, 329–342.
NEEM community members (2013), Eemian interglacial reconstructed from a Greenland folded ice core, *Nature*, *493*, 489–494.
Nicholl, J. A. L., et al. (2012), A Laurentide outburst flooding event during the last interglacial period, *Nat. Geosci.*, *5*, 901–904.
North Greenland Ice Core Project members (2004), High-resolution record of northern hemisphere climate extending into the last interglacial period, *Nature*, *431*(7005), 147–151.
Nürnberg, D., J. Bijma, and C. Hemleben (1996), Assessing the reliability of magnesium in foraminiferal calcite as a proxy for water mass temperatures, *Geochim. Cosmochim. Acta*, *60*, 803–814.
Obrochta, S. P., et al. (2014), Climate variability and ice-sheet dynamics during the last three glaciations, *Earth Planet. Sci. Lett.*, *406*, 198–212.
Oppo, D. W., J. F. McManus, and J. L. Cullen (2006), Evolution and demise of the last interglacial warmth in the subpolar North Atlantic, *Quat. Sci. Rev.*, *25*, 3268–3277.
Otto-Bliesner, B. L., et al. (2006), Simulating Arctic climate warmth and icefield retreat in the last interglaciation, *Science*, *311*(5768), 1751–1753.
Pausata, F. S., D. S. Battisti, K. H. Nisancioglu, and C. M. Bitz (2011), Chinese stalagmite controlled by changes in the Indian monsoon during a simulated Heinrich event, *Nat. Geosci.*, *4*(7), 474–480.
Peltier, W. R., and R. G. Fairbanks (2006), Global glacial ice volume and Last Glacial Maximum duration from an extended Barbados sea level record, *Quat. Sci. Rev.*, *25*(23), 3322–3337.
Pena, L. D., E. Calvo, I. Cacho, S. Eggins, and C. Pelejero (2005), Identification and removal of Mn-Mg-rich contaminant phases on foraminiferal tests: Implications for Mg/Ca past temperature reconstructions, *Geochem., Geophys., Geosyst.*, *6*, Q09P02, doi:10.1029/2005GC000930.
Pérez-Folgado, M., F. J. Sierro, J. A. Flores, J. O. Grimalt, and R. Zahn (2004), Paleoclimatic variations in foraminifer assemblages from the Alboran Sea (western Mediterranean) during the last 150 ka in ODP Site 977, *Mar. Geol.*, *212*(1), 113–131.
Pierre, C. (1999), The oxygen and carbon isotope distribution in the Mediterranean water masses, *Mar. Geol.*, *153*(1), 41–55.
Pross, J., U. Kotthoff, U. C. Müller, O. Peyron, I. Dormoy, G. Schmiedl, and A. M. Smith (2009), Massive perturbation in terrestrial ecosystems of the Eastern Mediterranean region associated with the 8.2 kyr BP climatic event, *Geology*, *37*(10), 887–890.
Rasmussen, S. O., et al. (2006), A new Greenland ice core chronology for the last glacial termination, *J. Geophys. Res.*, *111*, D06102, doi:10.1029/02005JD006079.
Reimer, P. J., E. Bard, A. Bayliss, J. W. Beck, P. G. Blackwell, C. Bronk Ramsey, and J. van der Plicht (2013), IntCal13 and Marine13 radiocarbon age calibration curves 0–50,000 years cal BP.
Rigual-Hernández, A. S., F. J. Sierro, M. A. Bárcena, J. A. Flores, and S. Heussner (2012), Seasonal and interannual changes of planktic foraminiferal fluxes in the Gulf of Lions (NW Mediterranean) and their implications for paleoceanographic studies: Two 12-year sediment trap records, *Deep-Sea Res.*, *66*, 26–40.
Rochon, A., A. D. Vernal, J. L. Turon, J. Matthießen, and M. J. Head (1999), Distribution of recent dinoflagellate cysts in surface sediments from the North Atlantic Ocean and adjacent seas in relation to sea-surface parameters, *Am. Assoc. Stratigraphic Palynologists Contrib. Ser.*, *35*, 1–146.
Rodrigo-Gámiz, M., F. Martínez-Ruiz, F. J. Jiménez-Espejo, D. Gallego-Torres, V. Nieto-Moreno, O. Romero, and D. Ariztegui (2011), Impact of climate variability in the western Mediterranean during the last 20,000 years: Oceanic and atmospheric responses, *Quat. Sci. Rev.*, *30*(15), 2018–2034.
Rodrigues, T., M. Rufino, C. Santos, E. Salgueiro, F. Abrantes, and P. Oliveira (2012), Iberian sea surface temperature calibration based in alkenones paleotemperature index Uk37. 7° Simpósio sobre a Margem Ibérica Atlantica, MIS.
Rogerson, M., E. Colmenero-Hidalgo, R. C. Levine, E. J. Rohling, A. H. L. Voelker, G. R. Bigg, and K. Garrick (2010), Enhanced Mediterranean-Atlantic exchange during Atlantic freshening phases, *Geochem., Geophys., Geosyst.*, *11*, Q08013, doi:10.1029/2009GC002931.
Rohling, E., and H. Pälike (2005), Centennial-scale climate cooling with a sudden cold event around 8,200 years ago, *Nature*, *434*, 975–979.
Rohling, E. J., et al. (2002), Rapid Holocene climate changes in the eastern Mediterranean, in *Droughts, Food and Culture*, edited by F. A. Hassan, pp. 35–46, Springer.
Rohling, E. J., R. H. Abu-Zied, J. S. L. Casford, A. Hayes, and B. A. A. Hoogakker (2009), The marine environment: Present and past, in *The Physical Geography of the Mediterranean*, edited by J. C. Woodward, pp. 33–67, Oxford Univ. Press, Oxford.
Ruddiman, W. F., and A. McIntyre (1981), Oceanic mechanisms for amplification of the 23,000-year ice-volume cycle, *Science*, *212*(4495), 617–627.
Sánchez-Goñi, M. F. S., M. F. Loutre, M. Crucifix, O. Peyron, L. Santos, J. Duprat, and J. P. Peypouquet (2005), Increasing vegetation and climate gradient in Western Europe over the Last Glacial Inception (122–110 ka): Data-model comparison, *Earth Planet. Sci. Lett.*, *231*(1), 111–130.
Sánchez-Goñi, M. F., et al. (2008), Contrasting impacts of Dansgaard-Oeschger events over a western European latitudinal transect modulated by orbital parameters, *Quat. Sci. Rev.*, *27*, 1136–1151.
Sánchez-Goñi, M. F., et al. (2012), European climate optimum and enhanced Greenland melt during the Last Interglacial, *Geology*, *40*(7), 627–630.
Sánchez-Goñi, M. F., et al. (2013), Air-sea temperature decoupling in western Europe during the last interglacial-glacial transition, *Nat. Geosci.*, *6*(10), 837–841.
Sánchez-Goñi, M. S., I. Cacho, J. L. Turon, J. Guiot, F. Sierro, J. Peypouquet, and N. Shackleton (2002), Synchroneity between marine and terrestrial responses to millennial scale climatic variability during the last glacial period in the Mediterranean region, *Clim. Dyn.*, *19*(1), 95–105.
Sbaffi, L., F. C. Wezel, N. Kallel, M. Paterne, I. Cacho, P. Ziveri, and N. Shackleton (2001), Response of the pelagic environment to palaeoclimatic changes in the central Mediterranean Sea during the Late Quaternary, *Mar. Geol.*, *178*(1), 39–62.
Schmittner, A., and E. D. Galbraith (2008), Glacial greenhouse-gas fluctuations controlled by ocean circulation changes, *Nature*, *456*(7220), 373–376.
Schrag, D. P., G. Hampt, and D. W. Murray (1996), Pore fluid constraints on the temperature and oxygen isotopic composition of the glacial ocean, *Science*, *272*(5270), 1930–1932.
Serrano, F., J. M. Gonzalez-Donoso, and D. Linares (1999), Biostratigraphy and paleoceanography of the Pliocene at Sites 975 (Menorca Rise) and 976 (Alboran Sea) from a quantitative analysis of the planktonicforaminiferal assemblages, in *Proceedings of the Ocean Drilling Program, Sci. Results*, vol. 161, edited by R. Zahn, M. C. Comas, and A. Klaus, pp. 185–195, Ocean Drilling Porgram, College Station, Tex.
Shackleton, N. J., M. A. Hall, and E. Vincent (2000), Phase relationships between millennial-scale events 64,000-24,000 years ago, *Paleoceanography*, *15*(6), 565–569, doi:10.1029/2000PA000513.
Siani, G., et al. (2001), Mediterranean sea surface radiocarbon reservoir age changes since the Last Glacial Maximum, *Science*, *294*(5548), 1917–1920.

Sicre, M. A., L. Labeyrie, U. Ezat, J. Duprat, J. L. Turon, S. Schmidt, and A. Mazaud (2005), Mid-latitude Southern Indian Ocean response to northern hemisphere Heinrich events, *Earth Planet. Sci. Lett.*, *240*(3), 724–731.
Siddall, M., E. J. Rohling, A. Almogi-Labin, C. Hemleben, D. Meischner, I. Schmelzer, and D. A. Smeed (2003), Sea-level fluctuations during the last glacial cycle, *Nature*, *423*(6942), 853–858.
Sierro, F. J., D. A. Hodell, J. H. Curtis, J. A. Flores, I. Reguera, E. Colmenero-Hidalgo, and M. Canals (2005), Impact of iceberg melting on Mediterranean thermohaline circulation during Heinrich events, *Paleoceanography*, *20*, PA2019, doi:10.1029/2004PA001051.
Skinner, L. C., and N. J. Shackleton (2006), Deconstructing Terminations I and II: Revisiting the glacioeustatic paradigm based on deep-water temperature estimates, *Quat. Sci. Rev.*, *25*, 3312–3321.
Skinner, L. C., N. J. Shackleton, and H. Elderfield (2003), Millennial-scale variability of deep-water temperature and $\delta^{18}O_{dw}$ indicating deep-water source variations in the Northeast Atlantic, 0–34 cal. ka BP, *Geochem., Geophys., Geosyst.*, *4*(12), 1098, doi:10.1029/2003GC000583.
Soulet, G., G. Ménot, G. Bayon, F. Rostek, E. Ponzevera, S. Toucanne, and E. Bard (2013), Abrupt drainage cycles of the Fennoscandian Ice Sheet, *Proc. Natl. Acad. Sci. U.S.A.*, *110*(17), 6682–6687.
Sprovieri, M., et al. (2012), Centennial- to millennial-scale climate oscillations in the Central-Eastern Mediterranean Sea between 20,000 and 70,000 years ago: Evidence from a high-resolution geochemical and micropaleontological record, *Quat. Sci. Rev.*, *46*, 126–135.
Sprovieri, R., E. Di Stefano, A. Incarbona, and M. E. Gargano (2003), A high-resolution record of the last deglaciation in the Sicily Channel based on foraminifera and calcareous nannofossil quantitative distribution, *Palaeogeogr. Palaeoclimatol. Palaeoecol.*, *202*(1), 119–142.
Stouffer, R. J., et al. (2006), Investigating the causes of the response of the thermohaline circulation to past and future climate changes, *J. Clim.*, *19*(8), 1365–1387.
Stuiver, M., and T. F. Braziunas (1993), Modeling atmospheric ^{14}C influences and ^{14}C ages of marine samples to 10,000 BC, *Radiocarbon*, *35*(1), 137–89.
Toucanne, S., S. Zaragosi, J. F. Bourillet, V. Marieu, M. Cremer, M. Kageyama, and P. L. Gibbard (2010), The first estimation of Fleuve Manche palaeoriver discharge during the last deglaciation: Evidence for Fennoscandian ice sheet meltwater flow in the English Channel ca 20–18 ka ago, *Earth Planet. Sci. Lett.*, *290*(3), 459–473.
van de Berg, W. J., M. van den Broeke, J. Ettema, E. van Meijgaard, and F. Kaspar (2011), Significant contribution of insolation to Eemian melting of the Greenland ice sheet, *Nat. Geosci.*, *4*(10), 679–683.
Van Nieuwenhove, N., and H. A. Bauch (2008), Last interglacial (MIS 5e) surface water conditions at the Vøring Plateau (Norwegian Sea), based on dinoflagellate cysts, *Polar Research*, *27*(2), 175–186.
Van Nieuwenhove, N., H. A. Bauch, F. Eynaud, E. Kandiano, E. Cortijo, and J. L. Turon (2011), Evidence for delayed poleward expansion of North Atlantic surface waters during the last interglacial (MIS 5e), *Quat. Sci. Rev.*, *30*(7), 934–946.
Van Nieuwenhove, N., H. A. Bauch, and H. Andruleit (2013), Multiproxy fossil comparison reveals contrasting surface ocean conditions in the western Iceland Sea for the last two interglacials, *Palaeogeogr. Palaeoclimatol. Palaeoecol.*, *370*, 247–259.
van Sebille, E., P. Scussolini, J. V. Durgadoo, F. J. C. Peeters, A. Biastoch, W. Weijer, C. Turney, C. B. Paris, and R. Zahn (2015), Ocean currents generate large footprints in marine palaeoclimate proxies, *Nat. Commun.*, *6*, 6521, doi:10.1038/ncomms7521.
Voelker, A. H. L., and L. de Abreu (2011), A review of abrupt climate change events in the Northeastern Atlantic Ocean (Iberian margin): Latitudinal, longitudinal and vertical gradients, *Geophys. Monogr. Ser.*, *193*, 15–37.
Von Grafenstein, R., R. Zahn, R. Tiedemann, and A. Murat (1999), Planktonic $\delta^{18}O$ records at Site 976 and 977, Alboran Sea: stratigraphy, forcing and paleoceanographic implications, in *Proceedings of the Ocean Drilling Program, Sci. Results*, vol. 161, edited by R. Zahn, M. C. Comas, and A. Klaus, pp. 469–479, Ocean Drilling Program, College Station, Tex.
Walker, M., et al. (2009), Formal definition and dating of the GSSP (Global Stratotype Section and Point) for the base of the Holocene using the Greenland NGRIP ice core, and selected auxiliary records, *J. Quat. Sci.*, *24*, 3–17, doi:10.1002/jqs.1227.
Wang, Y. J., et al. (2001), A high-resolution absolute-dated Late Pleistocene monsoon record from Hulu Cave, China, *Science*, *294*, 2345–2348.
Wang, Y., et al. (2005), The Holocene Asian monsoon: Links to solar changes and North Atlantic climate, *Science*, *308*(5723), 854–857.
Wang, Y., et al. (2008), Millennial and orbital scale changes in the east Asian monsoon over the past 224,000 years, *Nature*, *451*(7182), 1090–1093.
Wanner, H., et al. (2011), Structure and origin of Holocene cold events, *Quat. Sci. Rev.*, *30*(21–22), 3109–3123.
Weaver, A. J., O. A. Saenko, P. Clark, and J. X. Mitrovica (2003), Meltwater Pulse 1A from Antarctica as a trigger of the Bølling-Allerød warm interval, *Science*, *299*, 1709–1713.
Wit, J. C., G. J. Reichart, S. J. A. Jung, and D. Kroon (2010), Approaches to unravel seasonality in sea surface temperatures using paired single-specimen foraminiferal $\delta^{18}O$ and Mg/Ca analyses, *Paleoceanography*, *25*, PA4220, doi:10.1029/2009PA001857.
Yin, Q. Z., and A. Berger (2011), Individual contribution of insolation and CO_2 to the interglacial climates of the past 800,000 years, *Clim. Dyn.*, *38*(3–4), 709–724.
Yu, J., J. Day, M. Greaves, and H. Elderfield (2005), Determination of multiple element/calcium ratios in foraminiferal calcite by quadruple ICP-MS, *Geochem., Geophys., Geosyst.*, *6*, Q08P01, doi:10.1029/2005GC000964.
Yuan, D., et al. (2004), Timing, duration and transitions of the Last Interglacial Asian Monsoon, *Science*, *304*, 575–578.
Zahn, R., M. C. Comas, and A. Klaus (Eds.) (1999), *Proceedings of the Ocean Drilling Program, Sci. Results*, vol. 161, Ocean Drilling Program, College Station, Tex.
Zanchetta, G., R. N. Drysdale, J. C. Hellstrom, A. E. Fallick, I. Isola, M. K. Gagan, and M. T. Pareschi (2007), Enhanced rainfall in the western Mediterranean during deposition of sapropel S1: stalagmite evidence from Corchia cave (Central Italy), *Quat. Sci. Rev.*, *26*(3), 279–286.